The Journal of Physiology

J Physiol 601.7 (2023) pp 1265–1286

Dopamine differentially affects retinal circuits to shape the retinal code

Rebekah A. Warwick, Alina S. Heukamp, Serena Riccitelli and Michal Rivlin-Etzion

Department of Brain Sciences, Weizmann Institute of Science, 234 Herzl Street, Rehovot, Israel

Handling Editors: David Wyllie & Karin Dedek

The peer review history is available in the Supporting information section of this article (https://doi.org/10.1113/JP284215#support-information-section).

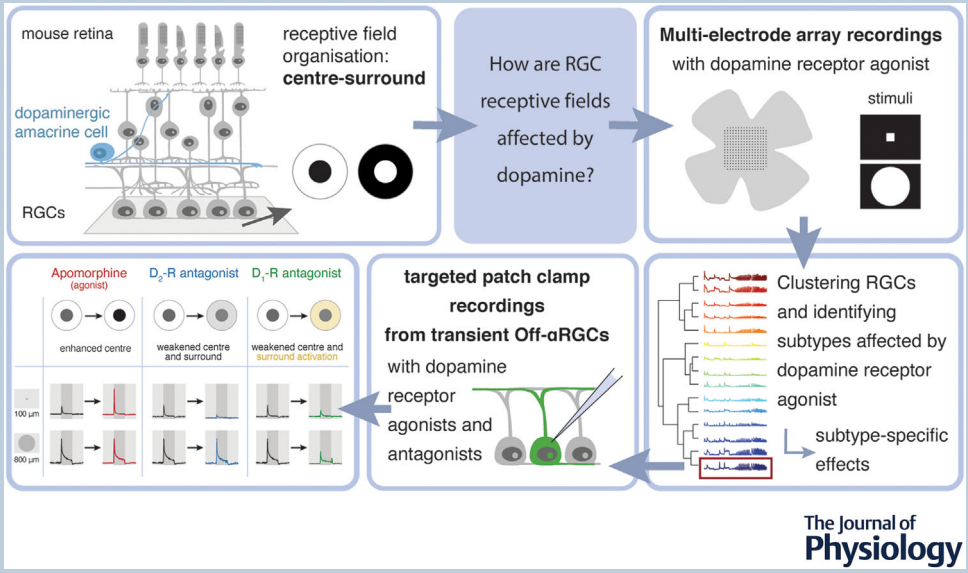

Abstract Dopamine has long been reported to enhance antagonistic surrounds of retinal ganglion cells (RGCs). Yet, the retina contains many different RGC subtypes and the effects of dopamine can be subtype-specific. Using multielectrode array (MEA) recordings we investigated how dopamine shapes the receptive fields of RGCs in the mouse retina. We found that the non-selective dopamine receptor agonist apomorphine can either increase or decrease RGCs' surround strength, depending on their subtype. We then used two-photon targeted patch-clamp to target a specific RGC subtype, the transient-Off-αRGC. In line with our MEA recordings, apomorphine did not increase the antagonistic surround of transient-Off-αRGCs but enhanced their responses to Off stimuli in the centre receptive field. Both D_1- and D_2-like family receptor (D_1-R and D_2-R)

Rebekah Warwick obtained her PhD at the Hebrew University of Jerusalem and conducted her post-doctoral research in Michal Rivlin's lab at the Weizmann Institute. She is interested in retinal computations and how they are affected by neuromodulators. **Alina Heukamp** obtained her MSc at the IMPRS for Neurosciences in Göttingen, Germany. She is currently a PhD student in the lab of Michal Rivlin and is interested in computations in the retina and beyond.

R. A. Warwick and A. S. Heukamp contributed equally to this work.

DOI: 10.1113/JP284215

blockers had the opposite effect and reduced centre-mediated responses, but differently affected transient-Off-αRGC's surround. While D_2-R blocker reduced surround antagonism, D_1-R blocker led to surround activation, revealing On responses to large stimuli. Using voltage-clamp recordings we separated excitatory inputs from Off cone bipolar cells and inhibitory inputs from the primary rod pathway. In control conditions, cone inputs displayed strong surround antagonism, while inputs from the primary rod pathway showed no surround. Yet, the surround activation in the D_1-R blockade originated from the primary rod pathway. Our findings demonstrate that dopamine differentially affects RGC subtypes via distinct pathways, suggesting that dopamine has a more complex role in shaping the retinal code than previously reported.

(Received 4 December 2022; accepted after revision 13 February 2023; first published online 17 February 2023)
Corresponding author M. Rivlin-Etzion: Department of Brain Sciences, Weizmann Institute of Science, 234 Herzl Street, Rehovot 7610001, Israel. Email: michal.rivlin@weizmann.ac.il

Abstract figure legend This study focuses on the receptive field organisation of retinal ganglion cells (RGCs), the output neurons of the retina (left). RGCs display a centre–surround receptive field organisation. Here, we asked how the neuromodulator dopamine, which is released by the dopaminergic amacrine cells, alters RGCs' receptive field organisation. We performed large-scale multi-electrode array recordings of RGCs while presenting visual stimuli in control conditions and in the presence of the dopamine receptor agonist apomorphine. After clustering RGCs into functional subtypes, we identified subtypes whose receptive field organisation is affected by apomorphine, and found that effects were subtype-specific. We then performed targeted patch-clamp recordings of an RGC subtype that was affected, the transient Off-αRGC, for a detailed characterisation of how dopamine shapes its receptive field.

Key points

- Receptive fields of retinal ganglion cells (RGCs) have a centre–surround organisation, and previous work has shown that this organisation can be modulated by dopamine in a light-intensity-dependent manner.
- Dopamine is thought to enhance RGCs' antagonistic surround, but a detailed understanding of how different RGC subtypes are affected is missing.
- Using a multielectrode array recordings, clustering analysis and pharmacological manipulations, we found that dopamine can either enhance or weaken antagonistic surrounds, and also change response kinetics, of RGCs in a subtype-specific manner.
- We performed targeted patch-clamp recordings of one RGC subtype, the transient-Off-αRGC, and identified the underlying circuits by which dopamine shapes its receptive field.
- Our findings demonstrate that dopamine acts in a subtype-specific manner and can have complex effects, which has implications for other retinal computations that rely on receptive field structure.

Introduction

The retina employs multiple strategies to operate over a large range of light levels (Fein & Szuts, 1982; Rivlin-Etzion et al., 2018; Shapley & Enroth-Cugell, 1984). Specialised rod and cone photoreceptors support vision across large ranges of light intensity, and horizontal cells, bipolar cells and amacrine cells exhibit functional changes as light intensity increases (Dunn et al., 2006, 2007; Flood & Eggers, 2021; Flood et al., 2018; Mazade & Eggers, 2013, 2016, 2020; Shapley & Enroth-Cugell, 1984; Xin & Bloomfield, 1999). Consequently, the output of retinal ganglion cells (RGCs) is also light intensity-dependent (Barlow et al., 1957; Dedek et al., 2008; Farrow et al., 2013; Pearson & Kerschensteiner, 2015; Tikidji-Hamburyan et al., 2015). A single signalling molecule, dopamine, has been credited with inducing many of these light-dependent changes (Flood et al., 2018; Godley & Wurtman, 1988; Goel & Mangel, 2021; Herrmann et al., 2011; Hu et al., 2010; Kothmann et al., 2009; Mazade et al., 2019). Dopamine is released from the dopaminergic amacrine cell and its levels increase with light intensity (Bauer et al., 1980; Godley & Wurtman, 1988; Pérez-Fernández et al., 2019; Witkovsky, 2004). Rod photoreceptors were shown to contribute to this process, suppressing release at low intensities and enhancing it at high light intensities (Pérez-Fernández et al., 2019).

All dopamine receptor subtypes are G-protein-coupled receptors, but activation of D_1-like family receptors (D_1-R) leads to an increase in cAMP, whereas activation of D_2-like family receptors (D_2-R) leads to a decrease in cAMP (Witkovsky 2004). D_1-Rs are expressed on horizontal, bipolar and amacrine cells (Farshi et al., 2016; Herrmann et al., 2011; Kothmann et al., 2009; Mazade & Eggers, 2020; Nguyen-Legros et al., 1999; Veruki & Wässle, 1996), and D_2-Rs are expressed on rod and cone photoreceptors as well as the dopaminergic amacrine cell (Muresan & Besharse, 1993; Veruki, 1997). RGCs have been reported to express both types (Koulen, 1999; Ogata et al., 2012; Tran et al., 2019; Single Cell Portal (SCP), Broad Institute). In all retinal cell types, the expression is selective to both cell subtype and receptor subtype. With dopamine receptors expressed throughout the retina, but dopaminergic amacrine cell processes mostly confined to the border of the inner plexiform and inner nuclear layers, the majority of dopamine signalling occurs in a paracrine fashion (Witkovsky, 2004).

A primary effect of dopamine on RGCs is to modulate their receptive field organisation. RGCs typically exhibit antagonistic centre–surround receptive fields, where the polarity of the surround is opposite to that of the centre. For example, a light stimulus presented solely in the centre of an On RGC's receptive field will elicit an On response. However, a light stimulus that includes its surround may have two effects: first, it may elicit an On response of reduced amplitude (a phenomenon termed 'surround antagonism', see Fig. 1*A*, top). Second, it may cause a response of opposite polarity to that of the centre, in this case an Off response (a phenomenon termed 'surround activation', see Fig. 1*A*, middle) (Chaffiol et al., 2017). RGCs with no surround will display similar responses to centre and full-field stimulation (Fig. 1*A*, bottom). Early studies investigating the effects of dopamine on RGCs' receptive fields found that blocking dopamine in light-adapted retinas weakened surround receptive fields (Jensen, 1991; Jensen & Daw, 1984, 1986). These studies were carried out on randomly selected RGCs that were clustered into groups based on their centre responses (On, Off and On–Off) and response kinetics (sustained or transient). Today we know that there are many more RGC subtypes, for example the mouse retina contains more than 30 different ones (Baden et al., 2016; Masland, 2012). Since each RGC subtype collects inputs from distinct sets of interneurons, different circuits may underlie their surround receptive fields (Farrow et al., 2013), and they may be differentially affected by dopamine.

Here, we used multielectrode array (MEA) recordings of RGCs to gain an understanding of how the dopamine receptor agonist apomorphine differentially shapes receptive fields of different subtypes of RGCs. After clustering RGCs into functional subtypes, we identified several subtypes that exhibit either a weakened or a strengthened surround with a dopamine receptor agonist. Guided by the results from our clustering, we then utilised the advancement of genetically labelled RGC subtypes to target one subtype, the transient-Off-αRGC (tOff-αRGC; Huberman et al., 2008). tOff-αRGCs receive input from Off cone bipolar cells and the primary rod pathway (Manookin et al., 2008). Using extracellular and intracellular recordings we found that apomorphine enhanced the centre response in tOff-αRGCs while having a differential effect on their surround, increasing surround antagonism of cone inputs but not of inputs from the primary rod pathway. Together, our findings suggest that dopamine's role in shaping RGC receptive fields is more complex than simply surround strengthening. Instead, dopamine's effects on centre–surround receptive fields are pathway-specific.

Methods

Ethical approval

All experimental procedures were approved by the Institutional Animal Care and Use Committee (IACUC) at the Weizmann Institute of Science (00860120-2).

Animals

Calb2-EGFP mice, in which tOff-αRGCs express green fluorescent protein (GFP), were obtained from Mutant Mouse Regional Resource Center (https://www.mmrrc.org/catalog/sds.php?mmrrc_id=283; Gong et al., 2003; Huberman et al., 2008) and crossed to C57BL/6JOlaHsd. The percentage of labelled tOff-αRGCs varied between the mice, and while some showed a mosaic of tOff-αRGCs, in others only a portion of them were labelled. For MEA recordings, wild-type mice from the same colony were used. Mice were kept on a 12:12 h light–dark cycle with free access to food and water. Mice of either sex were used.

Tissue preparation

Mice (4–20 weeks old) were deeply anaesthetised with isoflurane and decapitated. Retinas were isolated under dim red and infra-red illumination in oxygenated Ames' medium (Sigma-Aldrich, St Louis, MO, USA). The orientation of the retinas was based on landmarks in the choroid, as previously described (Wei et al., 2010).

For patch clamp recordings, dorsal retinas were isolated from the pigment epithelium and mounted photoreceptor side down over a hole of 1–1.5 mm^2 on filter paper, centred over the retina piece (GSWP01300, Merck Millipore, Billerica, MA, USA). Retinas were kept in the dark at room temperature in Ames' medium bubbled with 95% O_2–5% CO_2 until use (maximum 5 h).

For MEA experiments, the retina was mounted on a MEA as previously described (Warwick et al., 2022). In short, the MEA was coated with poly-D-lysine solution (PDL, 1.0 mg/ml in H_2O, Merck Millipore, CAT: A-003-E) for 1 h. After washing off the PDL, the dorsal half of the retina was mounted with the RGC layer facing the electrodes as previously described in Karamanlis et al. (2021).

MEA recordings

MEAs were purchased from MultiChannel Systems (Reutlingen, Germany; 252 electrodes, 8 μm electrode diameter, 30 μm minimal electrode distance, covering an area of 450 $\times$ 450 μm). The MEA was placed in the headstage with constant perfusion of oxygenated Ames' medium (flow rate: 3.5 ml/min) and a heating pad below maintained a temperature of 33.2°C. Data acquisition was started 1 h after placing the retina in the chamber to let the retina adapt. Extracellular voltage signals were amplified and digitised at 20 kHz and saved for offline analysis. In experiments where apomorphine (10 μM; cat. no. 2073, Tocris/Bio-Techne Ltd, Abingdon, UK) was used, a transistor-transistor logic (TTL) pulse was recorded to determine the time point of changing the solution. Apomorphine was washed in for 15 min before we presented visual stimuli again, and washed out for 30 min. Control experiments were performed in a similar way to study changes over time, but without adding any drug.

Light stimuli for MEA experiments

Visual stimuli were generated in a custom-written GUI in MATLAB (The MathWorks, Natick, MA, USA; Psychophysics Toolbox; Brainard, 1997; Pelli, 1997) and were projected via a monochromatic OLED display (eMagin, EMA-100309-01 SVGA+, 600 $\times$ 800 pixels, 60 Hz refresh rate) and focused on the photoreceptor layer via a telecentric lens (Edmund Optics, Barrington, NJ USA, $\times$2.0, no. 58-431), resulting in a pixel size of 7.5 μm on the retina. At maximum brightness, the irradiance was 2.6 μW/cm^2, resulting in 2.43 $\times$ 10^4 mouse rod isomerisations (R*rod^{-1} s^{-1}, corresponding to the photopic regime), whereas the minimum brightness was 70.4 R*rod^{-1} s^{-1}.

We presented several stimuli to probe the cells' centre–surround receptive field structure. For determining receptive fields, we presented a checkerboard white noise stimulus consisting of black and white squares of 60 μm size, changing at 30 Hz at equal probability, for 15 min. We used full-field spots (1200 μm diameter) and squares of different sizes (75 μm, 150 μm). We used full-field stimuli of three different contrasts: a white spot on black background, a white spot on grey background, and a black spot on grey background. Each of these consisted of 3 s background, 2 s presentation of the spot, followed by 3 s of background. The square stimulus consisted of white squares on a black background that were presented for 1 s in each position in a random order, one after the other. Squares of 75 μm size were presented in 196 different positions (on a 14 $\times$ 14 grid), and squares of 150 μm size were presented in 64 positions (on an 8 $\times$ 8 grid). For clustering the RGCs, we used a full-field stimulus consisting of contrast steps with each intensity presented for 2 s, followed by a contrast and frequency chirp (adapted from Baden et al., 2016; see Fig. 1*C*, top). To identify direction-selective cells, we presented moving square-wave gratings of 100% contrast with a spatial frequency of 397.5 μm, moving in eight equidistant directions in a pseudo-random order at a speed of 795 μm/s (2 Hz). All stimuli were preceded by 30 s background intensity to let the retina adapt. All stimuli (except for white noise) were presented for five repetitions.

Patch-clamp recordings

Retinas were placed under a two-photon microscope (Bruker, Billerica, MA, USA) equipped with a Mai-Tai laser (Spectra-Physics, Santa Clara, CA, USA) and superfused with oxygenated Ames medium at 32–34°C. Identification of and recording from GFP$^+$ cells was carried out as previously described (Rivlin-Etzion et al., 2011; Warwick et al., 2018). In short, GFP$^+$ cells were identified using the two-photon microscope laser at 920 nm to avoid bleaching of the photoreceptors. The inner limiting membrane above the targeted cell was dissected under the microscope with a glass electrode using infra-red illumination.

Loose-patch recordings (holding voltage set to 'off') were performed with a new glass electrode (3–5 MΩ) filled with Ames' medium. Intracellular voltage-clamp recordings were carried out using glass electrodes (6–8 MΩ) filled with intracellular solution containing (in mM): $CsMeSO_3$ 110, NaCl 2.8, HEPES 20, EGTA 4, TEA-Cl 5, ATP-Mg 4, GTP-Na_3 0.3, $C_4H_8N_3Na_2O_5P$ 10 and $C_{16}H_{27}N_2OBr$ 5; pH 7.35. A giga-ohm seal was obtained before breaking in. Data were acquired at 10 kHz and for whole-cell mode filtered at 2 kHz with a Multiclamp 700B amplifier (Molecular Devices, San Jose, CA, USA) using pCLAMP 10 recording software and a Digidata 1550 digitiser (Molecular Devices).

For experiments in which the drugs apomorphine (10 μM; cat. no. 2073, Tocris), raclopride (2.5 μM; cat. no. 1810, Tocris), SCH-23390 (1 μM; cat. no. 0925, Tocris) or L-2-amino-4-phosphonobutyric acid (L-AP4; 5 μM; cat. no. 0103, Tocris, UK) were used, and the relevant drug was added to the Ames solution and perfused for 30 min prior to recording from tOff-αRGCs. Stock concentrations of

drugs were prepared on the same day and stored at 4°C until use.

A portion of the data collected for the control condition in the loose patch and voltage-clamp experiments was previously published (Warwick et al., 2018).

Light stimuli for patch clamp experiments

Stimuli were generated using MATLAB and the Psychophysics Toolbox (Brainard, 1997; Pelli, 1997). A white, monochromatic organic light-emitting display (OLED-XL, 800 × 600 pixel resolution, 85 Hz refresh rate; eMagin, Bellevue, WA, USA) was used for the visual stimuli. The spectrum of the OLED was previously published (Warwick et al., 2018). The display image was projected through a ×20 water-immersion objective (UMPLFLN20xW; Olympus, Tokyo, Japan), via the side port of the microscope, centred on the soma of the recorded cell, and focused on the photoreceptor layer. The diameter of the entire display on the retina was 1 mm across. The visual stimulation consisted of a grey background for 2 s, followed by the appearance of a dark spot on the grey background, which lasted 2 s before the spot disappeared, leaving the same grey background for a further 2 s. Sizes of displayed spots ranged from 50 to 800 μm. Weber's contrast for the dark spot on the grey background was −0.85. The light intensity of the grey screen was 6.4×10^4 R*rod^{-1} s^{-1}. All retinas were kept in the dark until recording. After recording from one tOff-αRGC, the location of the next tOff-αRGC was chosen so that it had not been exposed to the light stimulus of the previous cell. A maximum of three cells were recorded from each retina.

Data analysis of MEA recordings

Spike sorting of MEA data was performed using Kilosort2.0 (Pachitariu et al., 2016, 2018) with manual curation in Phy (Rossant & Harris, 2013; Rossant et al., 2016). We only included well-separated units in our analysis, as determined by consistent spike shapes, spike amplitude, and inter-spike interval histogram that revealed a refractory period.

To determine RGCs' receptive field size and location, we calculated the spike-triggered average from the white noise data as the average stimulus preceding a spike, extracted from a time window of 500 ms before the spike in time steps of 20 ms. From the spike-triggered average, we extracted the stimulus frame with the highest peak-to-peak amplitude and fitted a 2D-Gaussian to the spatial component of the receptive field. The receptive field diameter was defined as 2 SD. The temporal component (shown in Fig. 1*C*) was extracted as the mean over all stimulus pixels included in the cell's receptive field centre. To find the position of the square (75 or 150 μm in size) that was closest to the cells' receptive field, we calculated the Euclidean distances between the centres of each presented square and the cells' receptive fields, and defined the 'centre square' as the square closest to the cell's receptive field centre (see Fig. 1*B*, bottom). From here on, we only considered the response to the square closest to each cell's receptive field centre.

Clustering of RGCs (described in the following section) was carried out on all non-direction selective RGCs. We calculated the normalised vector sum as $\mathrm{NVS} = \frac{|\Sigma R_\theta e^{i\theta}|}{\Sigma R_\theta}$, where R_θ represents the mean spike count in direction θ, and a direction-selectivity index (DSI) as $\mathrm{DSI} = \frac{R_{PD} - R_{ND}}{R_{PD} + R_{ND}}$, where R_{PD} represents the mean spike count in the preferred direction, defined as the direction closest to the angle of the normalised vector sum, and R_{ND} the response in the opposite direction. An orientation-selective index (OSI) was calculated as $\mathrm{OSI} = \frac{R_{PO} - R_{NO}}{R_{PO} + R_{NO}}$, where R_{PO} and R_{NO} are the spike counts in the preferred and null orientation, respectively. Direction-selective cells were defined as cells with a DSI $\geq$ 0.3, NVS $\geq$ 0.15, OSI $<$ 0.3 and mean firing rate $\geq$ 1 Hz in response to the grating stimulus, and were excluded in all further analyses.

To cluster RGCs into functional subtypes, we created a matrix of spike times consisting of the responses to different stimuli recorded in control conditions (no drug added). Out of the five repetitions, we only used responses from the third repetition. We concatenated the responses to the 150 μm square located closest to each cell's receptive field centre (On and Off response at onset and offset of the square respectively, 2 s combined), the response to the full-field contrast steps (consisting of five intensities of 2 s each) and the contrast and frequency-modulated full-field chirp. For each cell, we calculated a response quality index (RQI) from the peri-stimulus time histogram (PSTH; using a bin width of 50 ms) as $\mathrm{RQI} = \frac{\mathrm{Var}[R_r]_t}{\mathrm{Var}[R]_{tr}}$ (Baden et al., 2016), where R is the response matrix of stimulus repetitions × time bins, Var[] represents the variance and represents the mean over dimension t (time) or r (repetitions) as indicated. We only included responsive cells in our clustering algorithm, which we defined as cells with an RQI $\geq$ 0.35 and a Pearson correlation of the third repetition to its mean PSTH of $>$0.55. In total, we used 567 cells from nine retinas.

We used the SPIKY algorithm (Kreuz et al., 2013, 2015) to obtain a pairwise dissimilarity matrix between spike trains of all cells. We then performed agglomerative hierarchical clustering using the Ward distance to create a dendrogram. After analysing the merging cost between successive steps and visual inspection, as well as after excluding clusters with $<$20 cells, or clusters that contained cells from only a single retina, we obtained 15 functional clusters with distinct responses (Fig. 1*C*).

A second dataset of cells that were not presented with the chirp stimulus ($n = 847$ cells from 11 retinas) were then sorted into the existing clusters based on the Pearson correlation of their response to different full-field stimuli with the mean responses of each cluster. For that, we calculated the PSTHs (bin width of 5 ms) in response to a full-field spot of three different contrasts (a stimulus that was not used for the clustering, but was common to all cells). We then calculated the mean response of each cluster to the same stimuli and assigned each cell to the cluster with whose PSTH it had the highest correlation. Together, our final dataset included 1414 cells from 20 retinas.

After obtaining clusters, we could split each cluster into RGCs from apomorphine experiments and control experiments (no drug added) to study the effects of apomorphine on each cluster.

To calculate maximum firing rates, we calculated the PSTH in response to the full-field spot stimuli (three different contrasts, see above) and separated them into the On (light onset) and Off (light offset) response. For plots shown in Figs 1*D* and 2, we used the firing rate in response to the full-field stimulus onset or offset according to the cluster's preferred polarity (On or Off, respectively). We present responses to a white spot on black background for On responses (e.g. Fig. 2*A*–*C*), and responses to a black spot on grey background for Off responses (e.g. Fig. 2*G*–*I*). PSTHs and raster plots (Figs 1*A* and 2) are cropped to show 1 s of baseline before and after the spot. For the square stimulus, we considered the Off response as the response that occurred in 1 s after disappearance of the white square. For the example cells and clusters shown in Fig. 2, maximum firing rates are shown either during the On response (cluster no. 1; On cell), or the Off response (cluster no. 15; Off cell), or both (cluster no. 4; On–Off cell). An On–Off index (OOI) was calculated as $OOI = (R_{ON} - R_{OFF})/(R_{ON} + R_{OFF})$, where R_{ON} and R_{OFF} are the maximum firing rates during the On and Off response, respectively. This index was calculated for both square sizes and the full-field stimuli. For example, the example cell shown in Fig. 1*A* (middle) has an OOI > 0.3 in response to the centre 150 μm square stimulus, making it an On cell.

Spatial-selectivity indices (SSIs) were calculated as $SSI = (R_C - R_S)/(R_C + R_C)$, where R_C and R_S are the maximum firing rates during the centre and surround stimuli, respectively (Hoggarth et al., 2015). We calculated those values using maximal firing rates in response to the square stimuli (75 and 150 μm) as R_C, and the response to the full-field spot as R_S. We used the On or Off response according to each cluster's preferred polarity, determined by the OOI calculated in response to a full-field spot (white spot on black background; On response for OOI ≥ 0, Off response for OOI < 0, Fig. 1*E*).

To quantify the response kinetics, we calculated the ratio between the firing rate that occurred 200 ms after the maximum and the peak firing rate, resulting in values between 0 and 1, where high values correspond to prolonged, sustained responses and low values to short, transient responses. This was done for On and Off responses according to each cell's preferred polarity as explained above.

Data analysis of patch clamp recordings

Electrophysiological data were analysed offline. For loose-patch clamp recordings, spike times were extracted after filtration using a four pole Butterworth bandpass filter between 80 and 2000 Hz. PSTHs of spiking activity were calculated from five repetitions using a bin width of 50 ms. The background activity was determined based on the 2 s period of the initial grey screen in each trial and used to calculate the mean baseline activity and its SD. Cells were defined as responsive if their firing rate exceeded the mean baseline + 3 SD. The bin with the highest frequency during the dark spot stimulus was used to calculate the maximum response. For intracellular recordings, traces were averaged across four repeats. To quantify the response kinetics, we calculated the percentage of the peak response after 200 ms analogous to the MEA data.

The spatial selectivity index (SSI) was calculated as $(R_C - R_S)/(R_C + R_S)$ where R_C is the maximum firing rate of the centre response (defined as 50–400 μm) and R_S is the response to the largest stimulus (800 μm) (Hoggarth et al., 2015). Note that contrary to the MEA recordings, stimuli here are (a) centred on the cell's receptive field and (b) of a contrast that is preferred by tOff-αRGCs, so that values might differ between the two experimental set-ups, even for the same cell type.

Statistical analysis

For the MEA data, maximum firing rates and SSI values were compared using a two-tailed Wilcoxon signed rank test ($\alpha = 0.05$). For patch clamp data, a two-sample Student's t test was used to compare the mean SSI of the different groups.

A two-sample t test was used to compare the mean duration of Off responses for different groups. The Wilcoxon rank-sum test was used to compare groups of cells for each spot size. For comparisons in Fig. 5*H*, a Wilcoxon signed rank test was used. Statistical significance was accepted at $P < 0.05$.

Notation of P-values is according to $^{*}P < 0.05$, $^{**}P < 0.01$, $^{***}P < 0.001$, $^{****}P < 0.0001$. Numerical values are presented as means ± SD.

Results

Dopamine differentially affects RGC subtypes

To study whether dopamine differentially modulates the light responses of different RGC subtypes, we performed MEA recordings from adult dark-adapted mouse retinas. We used a white noise stimulus to determine the cells' receptive field (Chichilnisky, 2001), and both full-field spots (1200 μm diameter) and smaller square stimuli (75 and 150 μm square size presented at multiple locations, Fig. 1*B*) to estimate the surround strength. In order to study effects of dopamine in a more systematic manner, we clustered RGCs into functional subtypes using the SPIKY algorithm to calculate a pairwise dissimilarity matrix between spike trains of RGCs and a subsequent hierarchical clustering method (Jouty et al., 2018; Kreuz et al., 2013, 2015). For the clustering, we used responses to small squares (150 μm) and full-field (1200 μm) spots, as well as varying contrasts and frequency-modulated stimuli (full-field 'chirp' (Baden et al., 2016); see Methods). We obtained 15 functional clusters that were uniquely characterised by their light responses (Fig. 1*C*). RGCs that were recorded only in response to full-field spots of different contrasts were added to the existing clusters based on PSTH similarity (see Methods). The polarity preference of each cluster was defined based on the On–Off index (OOI) in response to a full field spot (see Methods), and in the analysis below we focussed on each cluster's preferred polarity response (On response for On cells, Off response for Off cells).

Next, we aimed to investigate how dopamine alters the receptive field organisation of different RGC subtypes. Dopamine has long been reported to strengthen RGCs' surround (Herlinger et al., 1995; Jensen, 1991; Jensen & Daw, 1984, 1986; Witkovsky, 2004). As dopamine is unstable in aqueous solutions (Herlinger et al., 1995), we chose to use apomorphine, a non-selective dopamine receptor agonist. At a concentration of 10 μM, apomorphine efficiently binds both D_1- and D_2-like family receptors despite having a higher affinity for the latter (Goldman & Kebabian, 1984). We investigated how application of apomorphine alters receptive fields of different clusters of RGCs. For that, we compared the maximum firing rates during small (75 and 150 μm) and full-field (1200 μm) stimuli in a control condition and after bath application of apomorphine. According to the classical view, dopamine-mediated increased surround antagonism would result in reduced firing rates in response to full-field spots (see example cell in Fig. 1*A*). Indeed, we found one cluster in which apomorphine significantly reduced maximum firing rates in response to full-field spots (Fig. 1*D*, cluster 1). We also found clusters with increased responses to full-field spots, suggesting a weakened surround (Fig. 1*D*, clusters 4, 5, 6 and 9). To quantify the relationship between centre and surround (full-field) responses, we calculated a spatial selectivity index (SSI; Hoggarth et al., 2015) as the normalised difference between each cell's centre and full-field responses, using either the On or Off response according to each cluster's preferred polarity (see Methods). SSI values range from −1 to 1. A value of 1 indicates strong surround antagonism, with complete suppression of the response to a full-field stimulus; a value of 0 indicates the absence of any antagonistic surround; and a negative value indicates a stronger response to the full-field stimulus compared to a centre stimulus. As expected from responses to centre and full-field stimuli, the SSIs of multiple clusters of RGCs were altered by apomorphine, revealing either enhancement or reduction in surround strength (Fig. 1*E*, clusters 1, 4, 6, 9, 12 and 15). In addition, we noticed that a few of the clusters changed the kinetics of their responses with apomorphine. We quantified the response decay as the ratio between the firing rate 200 ms after the peak and the maximum firing rate (see Methods). Four clusters showed a change in response decay with apomorphine, with clusters 3, 5 and 15 revealing a faster decay to the full-field stimulus and cluster 4 revealing a slower decay (Fig. 1*F*).

Cluster 1 provides an example of sustained On-RGCs that changed their centre–surround organisation with apomorphine (Figs 1*D–F* and 2*A–C*). Apomorphine reduced the maximum firing rate during the On response to the full-field spots (Fig. 2*A* and *C*; 103.8 ± 40.0 (before apomorphine, 'pre') *vs.* 89.9 ± 45.3 (with apomorphine, 'apo') spikes/s (mean ± SD, 1200 μm, $P = 0.005$)), suggesting a strengthened surround. The maximum firing rates during the small square stimuli were also reduced (Fig. 2*A* and *B*, 107.0 ± 54.5 *vs.* to 89.6 ± 49.7 spikes/s (150 μm, $P < 0.0001$), mean ± SD). Apomorphine did not significantly change the response decay of this cluster (see Supporting information). Here and in the following examples, effects of apomorphine were only partially washed out (after 30 min), probably due to long-lasting effects such as on gap-junction phosphorylation (Bloomfield & Völgyi, 2009; Goel & Mangel, 2021; Roy & Field, 2019).

In another cluster of non-direction selective On–Off RGCs (cluster 4, Figs 1*C* and 2*D–F*) we found the opposite effect. Here, the surround was weakened with apomorphine. RGCs in this cluster displayed an increased firing rate to full-field stimuli with apomorphine in the On and Off response, as well as increased responses to the 75 μm square stimulus (Fig. 2*D–F*, 34.4 ± 15.9 *vs.* to 49.8 ± 22.3 spikes/s (1200 μm, On response, $P = 0.006$); 27.6 ± 18.6 *vs.* 50.0 ± 29.0 spikes/s (1200 μm, Off response, $P < 0.0001$); 58.8 ± 32.1 *vs.* 87.1 ± 56.2 spikes/s (75 μm, On response, $P = 0.006$); 43.1 ± 32.2 *vs.* 59.7 ± 43.9 spikes/s (75 μm, Off response, $P = 0.031$); mean ± SD; see Supporting information). RGCs in this

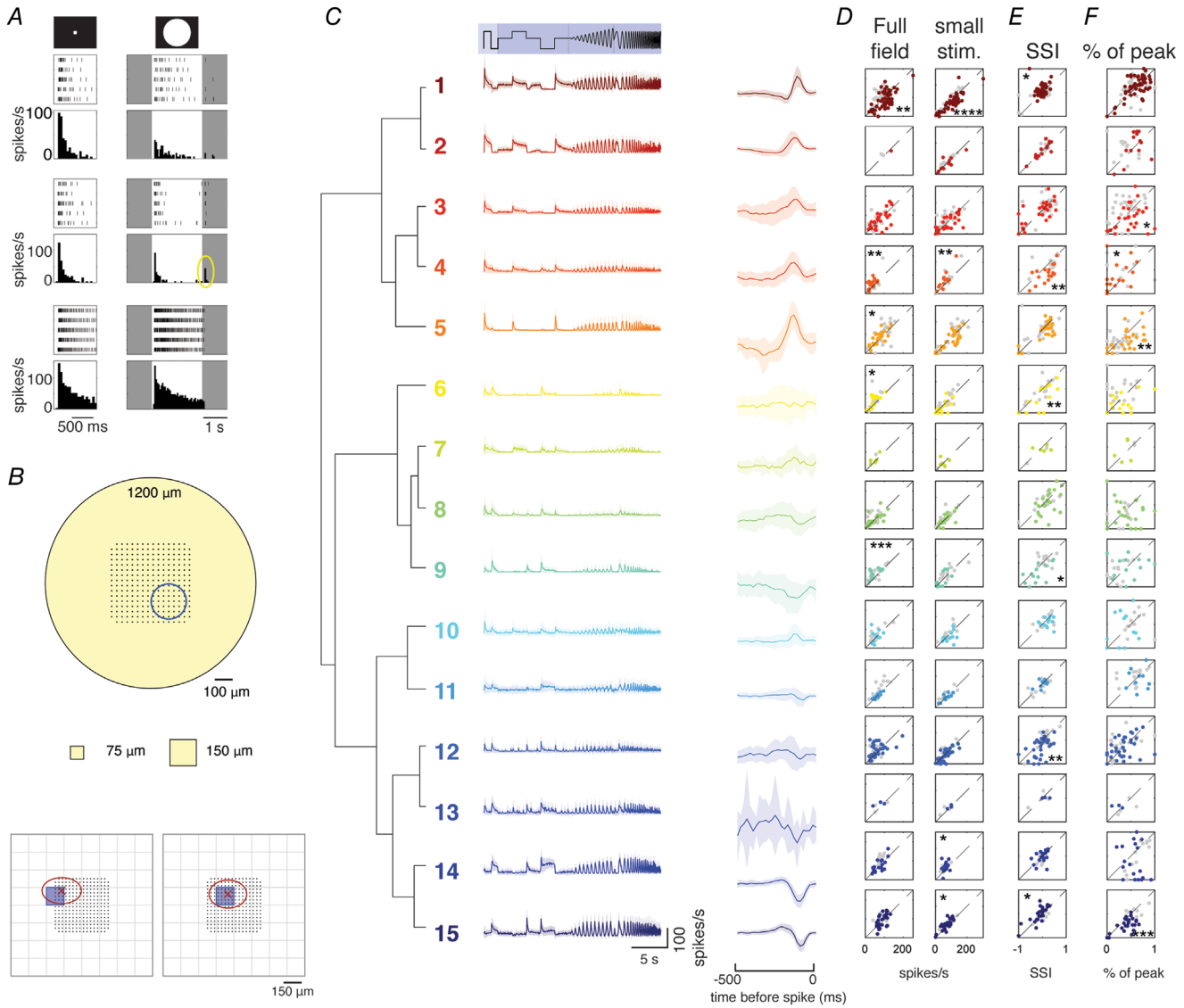

Figure 1. Clustering of RGCs into functional subtypes reveals complex effects of a dopamine receptor agonist on receptive field organisation
A, example of three different On-RGCs in response to a small (150 μm, left) and full-field (1200 μm, right) stimulus (shown in the first row). For each example, raster plots of 5 repetitions and PSTH are displayed. Top: a cell with a classical 'antagonistic surround'. Middle: a cell with 'surround activation' (note, this cell is an On cell (OOI for 150 μm square >0.3) that displays an Off response (yellow circle) to a full-field stimulus). Bottom: a cell with no surround. *B*, top: schematic representation of stimulus sizes used in MEA recordings. MEA is indicated by the black dots representing the electrodes. Blue circle shows an example receptive field with a diameter of 200 μm. Bottom: receptive field outlines (red) of two example cells on the MEA, showing the location of the 150 μm square (blue) closest to the cell's receptive field centre (red cross). Grey grid shows positions of all presented squares. *C*, left: functional clusters of RGC subtypes with their PSTH (mean $\pm$ SD). The stimulus is indicated above (light shaded: 150 μm, dark shaded: full-field). Right: temporal spike-triggered average (mean $\pm$ SD) to the white noise stimulus. Time below indicates time before spike. *D–F*, comparison of maximum firing rate to full-field spots (1200 μm, left) and the closest square stimulus (75 or 150 μm, right) to each cell's receptive field centre (*D*), spatial-selectivity index (SSI; *E*), and response decay for full-field stimuli (*F*) in pre condition (*x*-axis) *vs*. apomorphine (*y*-axis). For each cluster, the maximum firing rate was extracted from the On or Off response according to the cluster's preferred polarity (see Methods). Data points indicate individual RGCs. Control cells from the same cluster (without adding apomorphine) are shown in grey. Scales of *y*-axes are the same as *x*-axes (labelled below) for *D–F*. $^{*}P < 0.05$, $^{**}P < 0.01$, $^{***}P < 0.001$, $^{****}P < 0.0001$ according to the Wilcoxon signed rank test. Asterisks above and below the unity line indicate increases and decreases with apomorphine, respectively. [Colour figure can be viewed at wileyonlinelibrary.com]

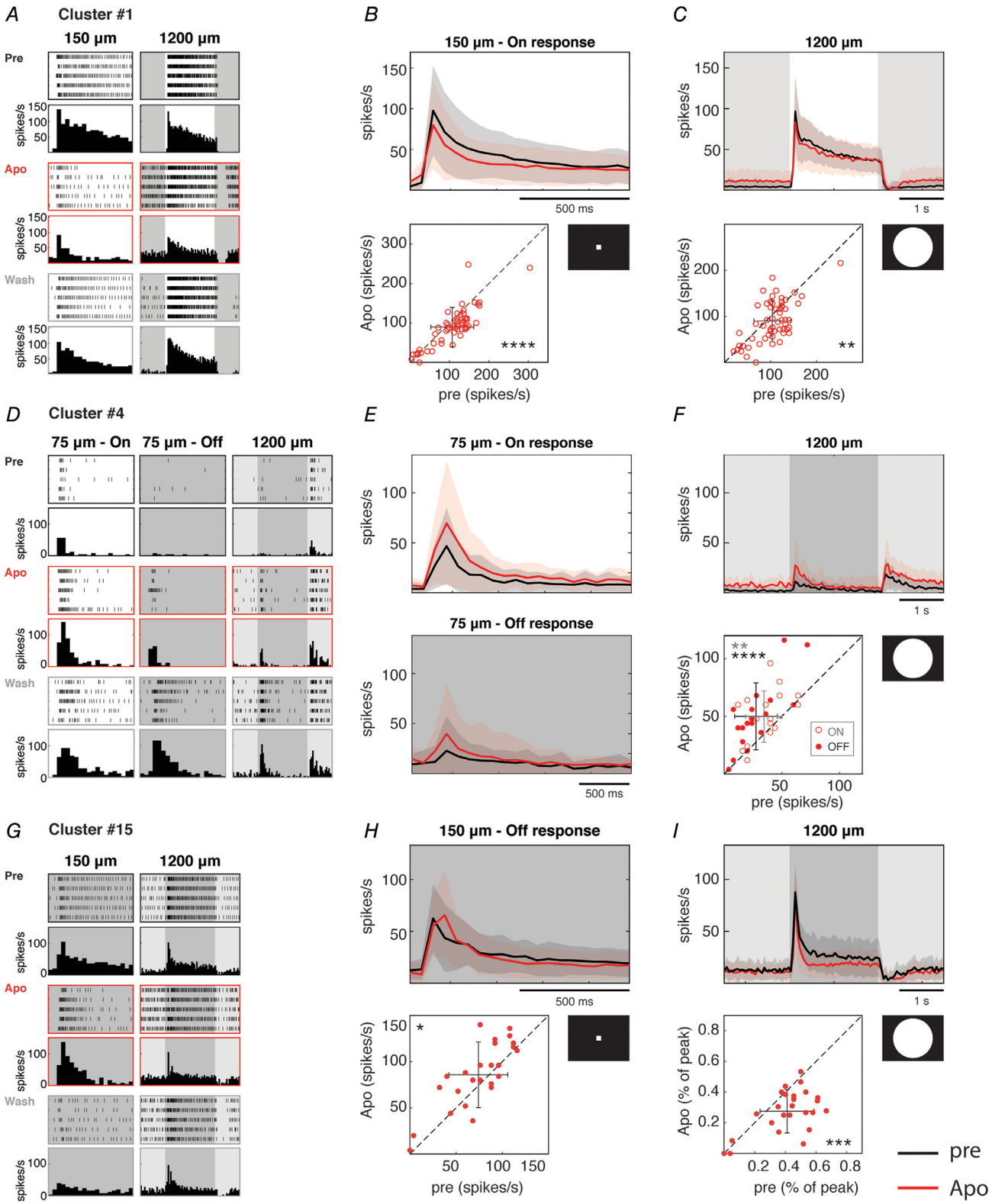

Figure 2. Apomorphine differentially affects responses to large *vs.* small stimuli in a subtype-specific manner
A, raster plot and mean PSTH of an example cell from cluster 1 (On cells) in response to the onset of a 150 μm square and a full-field stimulus (1200 μm) in pre condition (black frame), with apomorphine (red frame) and after washout (grey frame). *B*, top: mean ± SD PSTHs of all cells of cluster 1 (n = 57) in pre (black) and apomorphine

(red) conditions in response to a small stimulus. Bottom: maximum firing rate in response to the onset of the 150 μm square in pre condition (*x*-axis) and with apomorphine (*y*-axis) for all cells from this cluster. *C*, like *B* for the full-field response. *D*, like *A* for an example cell from cluster 4 (On–Off cells), showing the On and Off responses (white and grey background, respectively) to a 75 and 1200 μm stimulus. *E*, mean ± SD PSTH of On (top, white background) and Off (bottom, grey background) responses to a 75 μm spot for all cells from cluster 4 (n = 18 cells). *F*, like *C* with maximum firing rate during On and Off responses depicted by open and filled circles, respectively. *G*, like *A* for the Off responses of cluster 15 (Off cells, n = 25 cells). *H*, top: mean ± SD PSTH of Off responses to a 150 μm square offset. Bottom: maximum firing rate in response to offset of the square. *I*, top: mean ± SD PSTH in response to 1200 μm stimulus. Bottom: comparison of response kinetics (fraction of response 200 ms after peak) of Off response of the 1200 μm stimulus in pre condition (*x*-axis) and with apomorphine (*y*-axis). For population analysis, individual dots represent single cells. Mean ± SD are indicated in scatter plots. For *B*, *C*, *E*, *F*, *H* and *I*, asterisks above the unity line indicate increases with apomorphine and asterisks below indicate decreases. Colours of mean PSTHs as in the key at bottom right. $^{*}P < 0.05$, $^{**}P < 0.01$, $^{***}P < 0.001$, $^{****}P < 0.0001$ according to the Wilcoxon signed rank test. [Colour figure can be viewed at wileyonlinelibrary.com]

cluster also showed a change in their response kinetics with apomorphine, which was stimulus-size dependent. Specifically, responses to the disappearance of a small square (Off response) became more transient, whereas those to a full-field stimulus became more sustained (0.44 ± 0.24 *vs.* 0.21 ± 0.26 fraction of peak response (75 μm, Off response, $P = 0.025$); 0.21 ± 0.22 *vs.* 0.36 ± 0.29 (1200 μm, Off response, $P = 0.043$); mean ± SD; see Supporting information).

Finally, we observed a more complex phenomenon in cluster 15, where apomorphine enhanced responses to small stimuli but did not significantly change responses to full-field stimuli (Fig. 2*G–I*, 74.1 ± 31.8 *vs.* 85.8 ± 35.5 spikes/s (150 μm, Off response, $P = 0.015$); 88.6 ± 22.0 *vs.* 89.1 ± 34.7 spikes/s (1200 μm, Off response, $P = 0.919$); mean ± SD; see Supporting information), suggesting an enhanced centre response. With apomorphine, responses of these RGCs became more transient (Fig. 2*I* (bottom), 0.41 ± 0.18 *vs.* 0.28 ± 0.14 fraction of peak (1200 μm, Off response, $P = 0.0003$); mean ± SD). Based on their responses, we suspected that this cluster may correspond to cluster 8b from (Baden et al., 2016), the tOff-αRGCs. Overall, our findings suggest that dopamine can have a multitude of effects on RGC receptive field organisation, and can also influence their response kinetics.

Apomorphine facilitates tOff-αRGC light responses to small spot stimuli

Since we suspected that cluster 15 (Fig. 2*G–I*) corresponds to the well-studied tOff-αRGC (Krieger et al., 2017; Manookin et al., 2008; Münch et al., 2009; Murphy & Rieke, 2008; Pang et al., 2003; Wang et al., 2021; Warwick et al., 2018), we set out to gain a deeper understanding of how the dopamine receptor agonist apomorphine affects the centre–surround organisation of this RGC subtype. To this end, we conducted two-photon targeted patch clamp recordings of tOff-αRGCs labelled in the Calb2-EGFP transgenic mouse line (Huberman et al., 2008). To match our MEA experiments, and because we previously reported different activity patterns in the dorsal and ventral retina (Warwick et al., 2018), we exclusively recorded from cells in the dorsal retina. The light stimulus consisted of a dark spot centred on the cell soma, appearing for 2 s on a grey background. In order to examine the receptive field properties, we used a variety of spot sizes, ranging from 50 to 800 μm in diameter (Fig. 3*A*; see Methods).

To start with, we characterised the light responses of tOff-αRGCs under control conditions (Fig. 3*B*). These cells displayed an Off response to the dark spots and had a peak maximum firing rate to the 300 μm spot, after which the maximum firing rate decreased for increasing spot size. This decrease is mediated by surround antagonism, which is known to be weak but apparent in tOff-αRGCs (Farrow et al., 2013; Warwick et al., 2018). As for the MEA data, we quantified the surround antagonism using the SSI (Hoggarth et al., 2015; see Methods). Control tOff-αRGCs had an SSI of 0.19 ± 0.11 (mean ± SD) due to their weak antagonistic surrounds. Next, we repeated the experiments in the presence of apomorphine (10 μM) to mimic the effect of increasing dopamine levels in the retina (Fig. 3*C*). Apomorphine did not increase the surround antagonism (SSI of 0.19 ± 0.11 (pre) *vs.* 0.17 ± 0.07 (apo), $P = 0.518$). However, similarly to the effects on cluster 15, the dopamine receptor agonist did facilitate tOff-αRGC responses, significantly increasing their maximum firing rates to the smallest spot sizes (50–200 μm spots; Fig. 3*C–E*). Moreover, apomorphine tended to shorten the responses of tOff-αRGCs, and this was significant for the smallest spot sizes (50–200 μm spots; Fig. 3*F*). These findings suggest that dopamine can enhance centre-mediated responses in tOff-αRGCs and change their response kinetics.

In order to investigate how reduced levels of dopamine affect the receptive field properties of tOff-αRGCs, we used dopamine receptor antagonists (Fig. 4). Raclopride (2.5 μM) was used to inhibit D_2-R, and SCH-23390 (1 μM) was used to inhibit D_1-R. Under D_2-R blockade, surround antagonism was abolished (SSI of 0.19 ± 0.11 (pre) *vs.* −0.01 ± 0.20 (D_2-R block), $P = 0.008$).

No significant difference was observed between the SSI of tOff-αRGCs under control conditions and blockade of D_1-R (0.19 $\pm$ 0.11 *vs.* 0.06 $\pm$ 0.28, $P = 0.098$). However, antagonists for both D_2-R and D_1-R reduced Off responses to the smaller spot sizes (Fig. 4*B*–*E*). Blockade of D_2-R significantly reduced the maximum firing rates of tOff-αRGCs in response to the 200 and 300 μm spots (Fig. 4*D*), and blockade of D_1-R significantly reduced the maximum firing rates in response to the 200–500 μm spots (Fig. 4*E*).

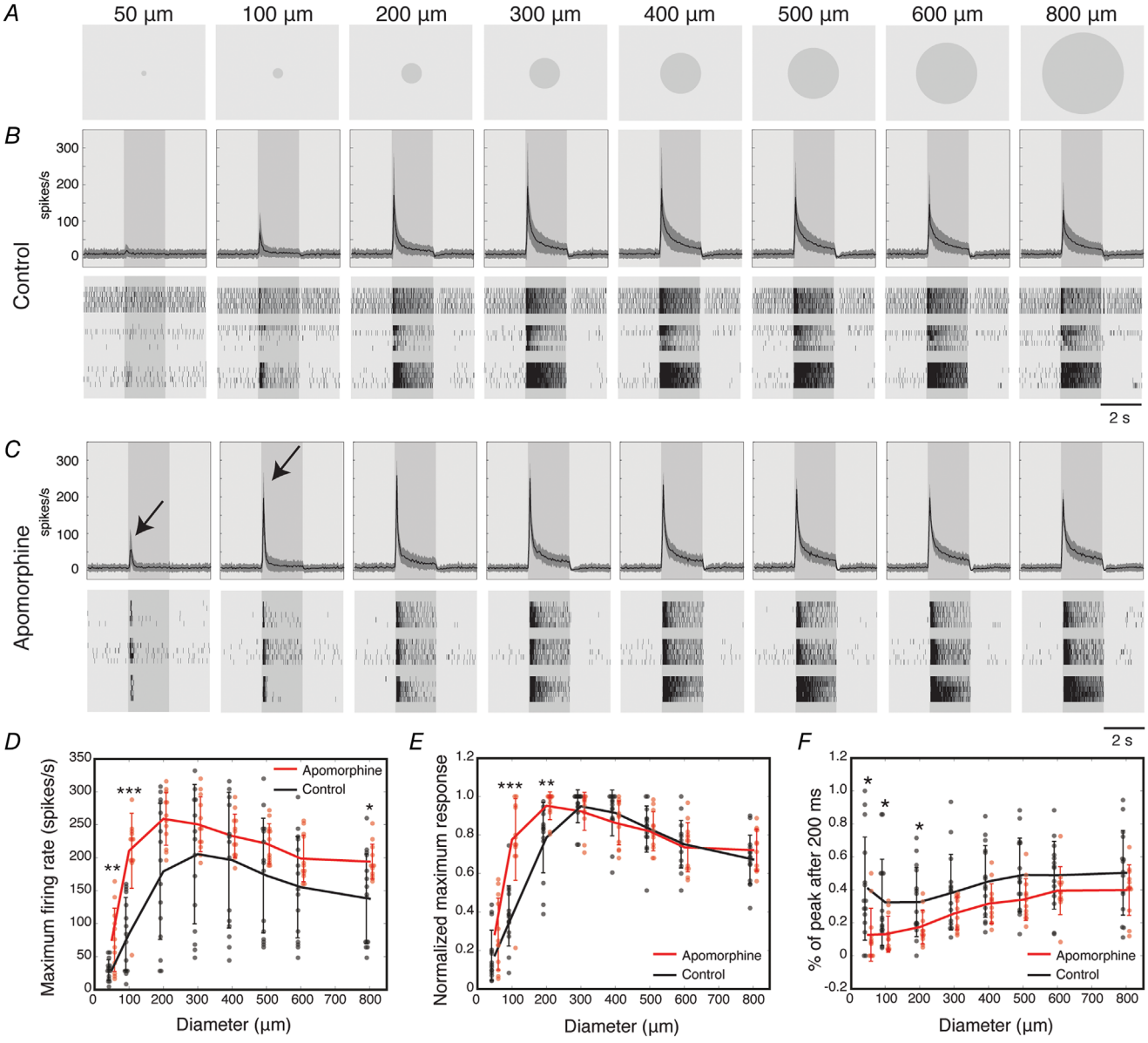

Figure 3. Apomorphine does not enhance surround antagonism but increases firing rates of tOff-αRGCs in response to small spot stimuli
A, diagram illustrating the different sized spots used as light stimuli. *B* and *C*, top: mean $\pm$ SD firing rate of tOff-αRGCs under control conditions (*B*) and in the presence of apomorphine (10 μM; *C*). Arrows indicate increased response to small spot stimuli with apomorphine. Bottom: raster plots of three example tOff-αRGCs. Each row corresponds to 5 repeats of the stimulus. *D*, maximum firing rate (spikes/s) as a function of spot size for control tOff-αRGCs (black) and tOff-αRGCs in the presence of apomorphine (red). *E*, normalised maximum response as a function of spot size for control tOff-αRGCs (black) and tOff-αRGCs in the presence of apomorphine (red). *F*, response decay quantified as the fraction of the maximum firing rate 200 ms after the peak. n = 15 tOff-αRGCs from 15 mice for control conditions, n = 12 tOff-αRGCs from five mice in the presence of apomorphine. For *D*–*F*, dots represent single cells. Error bars represent the mean $\pm$ SD. Dots and error bars were offset/jittered for legibility. $^*P < 0.05$, $^{**}P < 0.01$, $^{***}P < 0.001$ according to the Wilcoxon rank-sum test. [Colour figure can be viewed at wileyonlinelibrary.com]

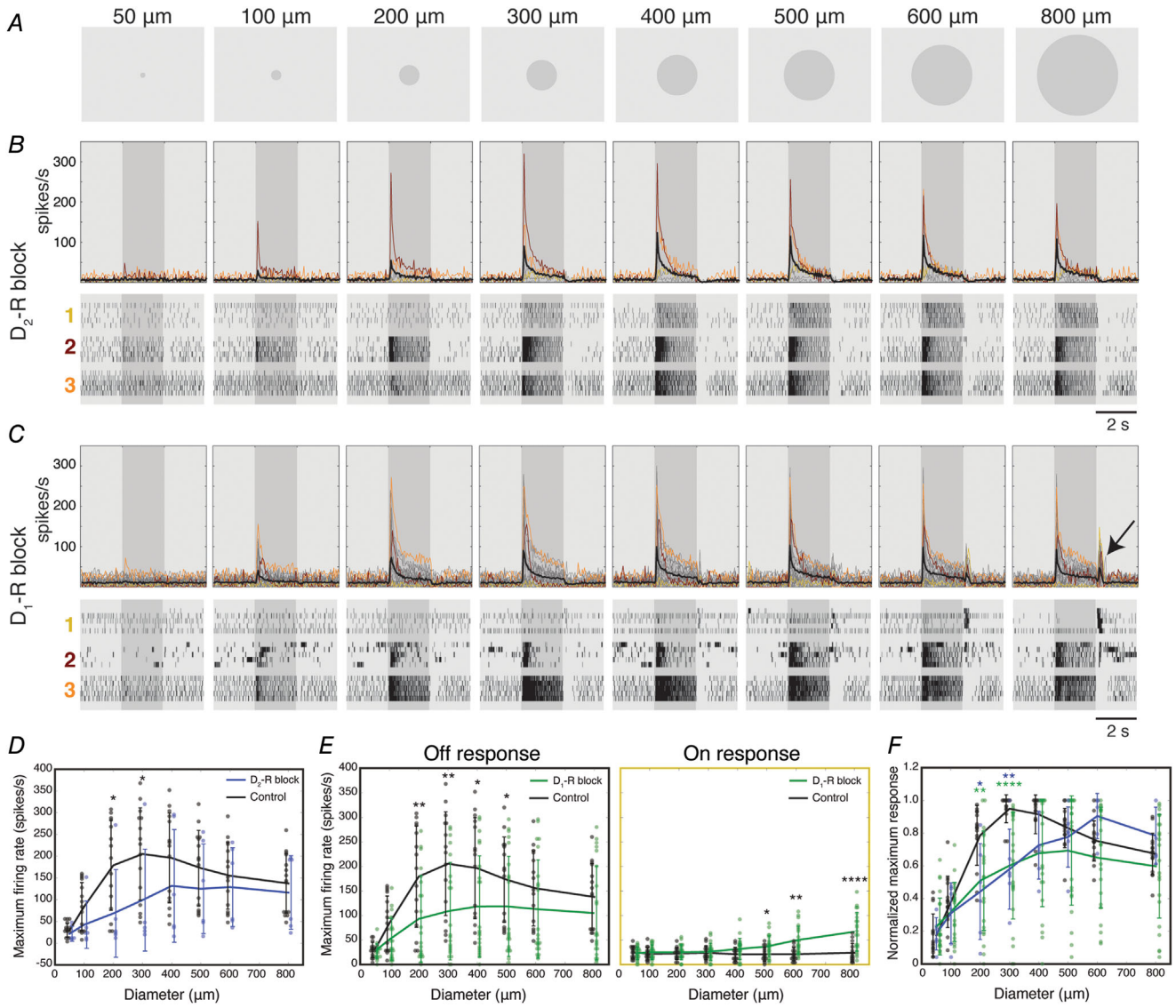

Figure 4. Blockade of both D_2-R and D_1-R reduces Off responses to small spot stimuli, but only D_1-R blockade causes On responses to large spot stimuli
A, diagram illustrating the different sized spots used as light stimuli. *B* and *C*, firing rate and raster plots of tOff-αRGCs under blockade of D_2-R (*B*) and D_1-R (*C*). Individual PSTHs are shown in grey, except for the three examples shown in the raster plots below, which are indicated by the numbers on the left. Mean PSTH is overlaid in black. Arrow indicates surround-activation On response with D_1-R blocker. For *C*, the example raster plots display two extreme cases of a cell with diminished Off response (cell 1) and a cell with no On response (cell 3), together with a representative cell, which maintained its Off response alongside revealing an On response (cell 2). *D*, maximum firing rate (spikes/s) as a function of spot size for control tOff-αRGCs (black) and tOff-αRGCs under D_2-R blockade (*D*, blue). *E*, maximum firing rate (spikes/s) for the Off (left) and On (right) responses as a function of spot size for control tOff-αRGCs (black) and under D_1-R blockade (green). *F*, normalised maximum Off response as a function of spot size for control tOff-αRGCs (black line), tOff-αRGCs under D_2-R (blue line) and D_1-R blockade (green line). Colours match *D* and *E*. $n = 15$ tOff-αRGCs from 15 mice for control conditions, $n = 6$ tOff-αRGCs from six mice for D_2-R blockade, $n = 22$ tOff-αRGCs from 16 mice for D_1-R blockade. For *D*–*F*, dots represent single cells. Error bars represent the mean ± SD. Dots and error bars were offset/jittered for legibility. $^*P < 0.05$, $^{**}P < 0.01$, $^{****}P < 0.0001$ according to the Wilcoxon rank-sum test. [Colour figure can be viewed at wileyonlinelibrary.com]

As apomorphine affected the firing rates of tOff-αRGCs, we normalised each individual tOff-αRGC to its overall maximum firing rate in order to compare receptive field shape between the different groups (Figs 3*E* and 4*F*). Under control conditions, tOff-αRGCs responded maximally to the 300 μm spot. The dopamine receptor agonist apomorphine shifted the maximum response to a smaller spot size of 200 μm (Fig. 3*E*), whereas the D_2-R and D_1-R antagonists shifted it to larger spots of 600 and 500 μm, respectively (Fig. 4*F*). These data suggest that dopamine may affect the receptive field organisation of tOff-αRGCs by increasing the centre Off response to smaller stimuli.

D_1-R blockade reveals On responses in tOff-αRGCs

We recorded from a total number of 22 tOff-αRGCs under D_1-R blockade. Interestingly, they did not change only their Off responses under this condition. Examination of their responses revealed a transient On response to the disappearance of the larger dark spots, most notably the 800 μm spot (Fig. 4*C*). The maximum firing rates during light onset (2 s following the dark spot disappearance) revealed that this On response emerged for the spots sized 500–800 μm compared with control tOff-αRGCs (Fig. 4*E*, right). In total, 16 out of 22 tOff-αRGCs displayed a significant increase in firing rate after the disappearance of the black spot. We observed some variability in the responses of tOff-αRGCs under D_1-R blockade (Fig. 4*C*) that may be due to differences in the underlying circuits, which vary with location along the ventral–dorsal retinal axis in a gradual manner (Warwick et al., 2018). Another possible source of variability can be different drug incubation times (see Discussion).

Some cells that exhibited On responses had decreased or even absent Off responses (Fig. 4*C*). Comparing control tOff-αRGCs to the tOff-αRGCs subpopulation that exhibited On responses under D_1-R blockade revealed a significant decrease in the Off response duration to the 800 μm spot from 1287 $\pm$ 581 to 538 $\pm$ 720 ms (mean $\pm$ SD, $P = 0.004$). For the 6/22 cells that did not exhibit On responses, we observed no decrease in Off response duration to the 800 μm spot (1808 $\pm$ 139 ms). This suggests that the On and Off responses are mediated by opposing mechanisms. As opposed to the Off response, which decreased to the smaller spot stimuli, the On response under D_1-R blockade emerged at large stimuli (500 μm) and increased with spot size (Fig. 4*E*, right), suggesting that these On responses resulted from surround activation. We next aimed at revealing the source for these On responses in tOff-αRGCs.

The tOff-αRGC is known to receive synaptic input from both the Off and On pathways. While the tOff-αRGC receives glutamatergic (excitatory) input from the Off pathway via Off cone bipolar cells and potentially from vGlut3 amacrine cells (Kim et al., 2020; Lee et al., 2016), it also receives glycinergic (inhibitory) input from the On pathway via AII amacrine cells. These AII amacrine cells depolarise during light onset as they are excited by rod bipolar cells (forming the primary rod pathway; Murphy & Rieke, 2008; van Wyk et al., 2009) and are gap-junction coupled to On cone bipolar cells (Fig. 5*A*) (Beaudoin et al., 2008; Demb & Singer, 2012; Manookin et al., 2008; Münch et al., 2009; Murphy & Rieke, 2006). As a result, tOff-αRGCs are activated during light offset in a push–pull mechanism, excited by Off bipolar cells (via the Off pathway) and at the same time disinhibited by AII amacrine cells (via the On pathway) (Manookin et al., 2008; van Wyk et al., 2009). Previously, it was thought that rods are saturated at photopic light levels and do not contribute to the processing of light information under high illumination conditions. However, recent work has shown that this is not the case (Szikra et al., 2014; Tikidji-Hamburyan et al., 2017; Vlasits et al., 2014), leading us to speculate that the On responses we detected in tOff-αRGCs could arise from the primary rod pathway.

To establish whether the On pathway was indeed responsible for the On responses detected in tOff-αRGCs in the presence of D_1-R blockade, we selectively blocked the On pathway by adding L-AP4 (5 μM), a selective group III metabotropic glutamate receptor agonist, to the Ames solution (Fig. 5*B*). None of the 5/5 tOff-αRGCs examined displayed an On response to large spots in the presence of a D_1-R-antagonist and L-AP4 (Fig. 5*C*–*G*), confirming that the On pathway was responsible for the observed On responses in tOff-αRGCs during D_1-R blockade. Two other observations were made during L-AP4 application. Firstly, the combination of the D_1-R antagonist + L-AP4 increased the background firing activity compared to the D_1-R antagonist alone from 8.5 $\pm$ 8.6 to 36.7 $\pm$ 24.4 spikes/s (mean $\pm$ SD, $P = 0.041$; Fig. 5*D*–*G*). Under control conditions, tOff-αRGCs are known to receive tonic inhibition from AII amacrine cells (Manookin et al., 2008). Although the increase in background activity in the presence of D_1-R antagonist + L-AP4 may suggest that tonic inhibition exists under D_1-R antagonist alone, whether this is indeed the case is not known. Note that the high background activity observed under D_1-R antagonist + L-AP4 is responsible for the relatively high firing rates during light onset in Fig. 5*G* (yellow line), which does not correspond to actual light responses. Secondly, tOff-αRGCs had higher maximum firing rates to the appearance of the dark spot (light offset) in the presence of the D_1-R-antagonist + L-AP4 compared to the D_1-R-antagonist alone (Fig. 5*H*). L-AP4 alone is expected to decrease Off responses in tOff-αRGCs via the loss of the 'push–pull' mechanism (Manookin et al., 2008). Our results suggest that D_1-R blockade compensates for this decrease, either via enhancing

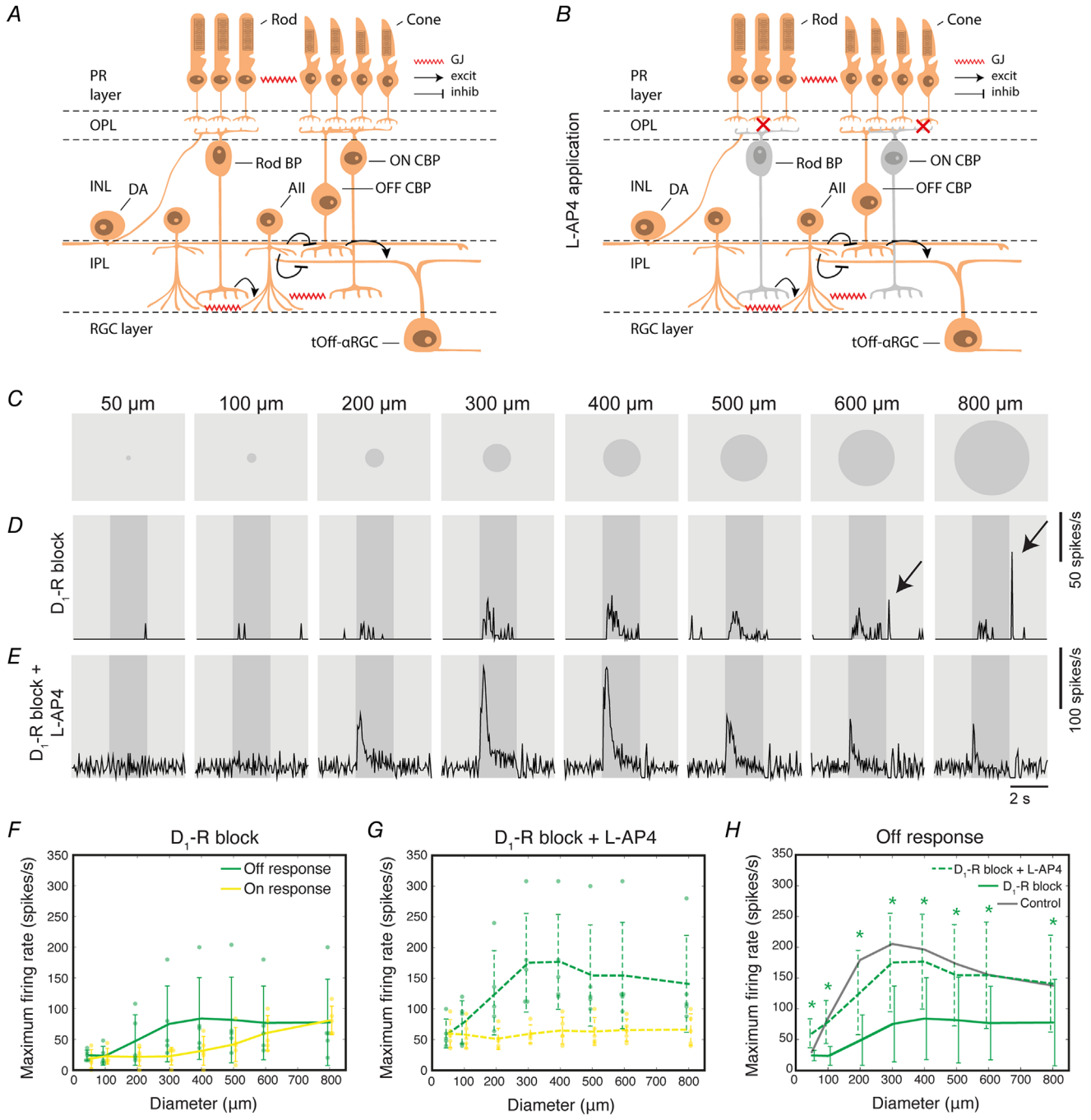

Figure 5. The On pathway mediates On responses in tOff-αRGCs under D_1-R blockade
A, diagram illustrating the main pathways underlying the response in tOff-αRGCs. BP, bipolar; CBP, cone bipolar; DA, dopaminergic amacrine cell; excit, excitation; GJ, gap junction; inhib, inhibition; INL, inner nuclear layer; IPL, inner plexiform layer; OPL, outer plexiform layer; PR, photoreceptor. *B*, same as in *A* except after L-AP4 application. *C*, diagram illustrating the different sized spots used as light stimuli. *D* and *E*, mean firing rate of an example tOff-αRGC under D_1-R blockade (*D*) and after addition of L-AP4 (*E*). On responses (indicated by arrows) disappeared with L-AP4. *F* and *G*, maximum On (yellow) and Off (green) firing rates as a function of spot size under D_1-R blockade prior to addition of L-AP4 (*F*) and following addition of L-AP4 (5 μM) (*G*). *H*, maximum Off firing rates as a function of spot size for the 5 tOff-αRGCs before and after the addition of L-AP4 while under D_1-R blockade. Maximum firing rates under control conditions are shown for comparison (black). Control (black) is taken from Figs 3 and 4 for comparison. Asterisks indicate significant difference between D_1-R blockade before and after addition of L-AP4. $n = 5$ tOff-αRGCs from four mice for D_1-R blockade and after the addition of L-AP4. $n = 15$ tOff-αRGCs from 15 mice for control conditions. For *F*–*H*, dots represent single cells. Error bars represent mean ± SD. Dots and error bars were offset/jittered for legibility. $^*P < 0.05$ according to the Wilcoxon signed rank test. [Colour figure can be viewed at wileyonlinelibrary.com]

tOff-αRGCs Off-pathway input or via another unknown pathway.

D_1-R blockade has differential effects on the multiple pathways underlying the tOff-αRGC response

In order to establish how the different circuits underlying the tOff-αRGC response are affected under D_1-R blockade, we conducted whole-cell voltage-clamp recordings (Fig. 6). Voltage-clamping the tOff-αRGC at 0 mV and −60 mV allowed us to separate the inhibitory and excitatory inputs, respectively. The AII amacrine cell is considered the main inhibitory presynaptic partner to the tOff-αRGC, but other inhibitory cells may contribute. Off cone bipolar cells are considered the main excitatory presynaptic partners to the tOff-αRGC. Note that AII amacrine cells can also influence the glutamatergic input onto the tOff-αRGC by forming glycinergic synapses onto the Off cone bipolar cells (Fig. 5*A*) (Manookin et al., 2008; Murphy & Rieke, 2008; Warwick et al., 2018).

Examining the excitatory input to tOff-αRGCs under control conditions revealed a transient and a sustained component during light offset (Fig. 6*B*). The transient component, which is thought to originate from cone pathways (Warwick et al., 2018), peaked in response to the 200 μm spot and disappeared entirely for the 800 μm spot,

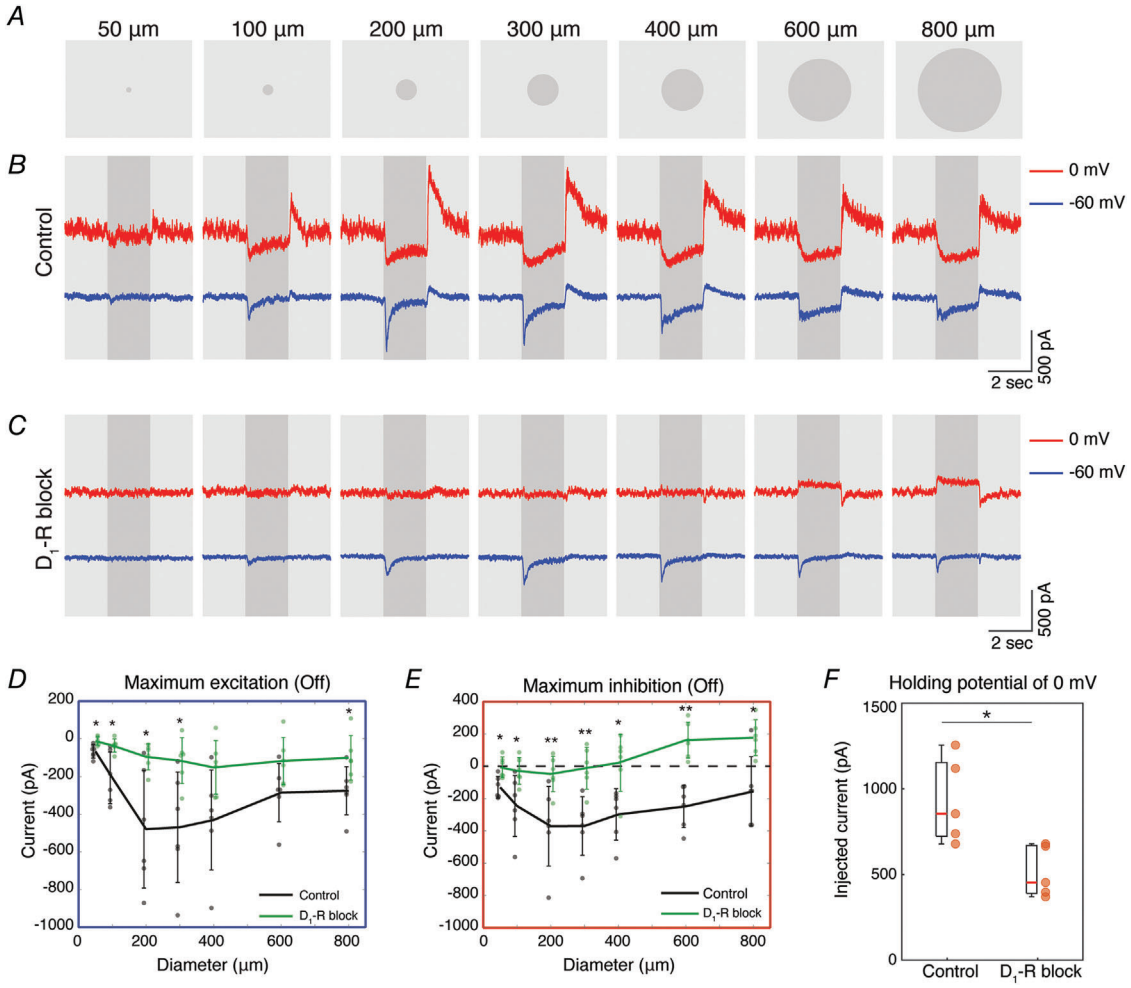

Figure 6. D_1-R blockade differentially affects the inhibitory and excitatory inputs onto the tOff-αRGC
A, diagram illustrating the different sized spots used as light stimuli. *B–C*, current traces of an example control tOff-αRGC (*B*) and an example tOff-αRGC under D_1-R blockade (*C*) when held at 0 (red) and −60 (blue) mV. *D*, maximum excitatory current during Off stimulus as a function of spot size for control tOff-αRGCs (black line) and tOff-αRGC under D_1-R blockade (green line). *E*, same as *D*, maximum for inhibitory current. *F*, box plots and data points for the injected current needed to hold the cell at 0 mV from the resting potential during the presentation of the grey background for control tOff-αRGCs and tOff-αRGCs under D_1-R blockade. For *D* and *E*, $n = 6$ tOff-αRGCs. For *F*, $n = 5$ tOff-αRGCs from five mice for control conditions, $n = 5$ tOff-αRGCs from three mice for D_1-R blockade. For *D–F*, dots represent single cells. Error bars represent the mean ± SD. Dots and error bars were offset/jittered for legibility. $^*P < 0.05$, $^{**}P < 0.01$ according to the Wilcoxon rank-sum test. [Colour figure can be viewed at wileyonlinelibrary.com]

suggesting it is susceptible to strong surround antagonism. This is in contrast to D_1-R blockade where the transient excitation peaked at the 400 μm spot and was still present in response to the 800 μm spot, suggesting weaker surround antagonism (Fig. 6*C* and *D*). The maximum excitatory currents were significantly reduced for the 50–300 μm spots under D_1-R blockade (Fig. 6*D*). This reduction in excitation could contribute to the lower firing rates observed during the extracellular recordings (Fig. 4*E*).

The sustained excitatory component present under control conditions is likely the result of AII glycinergic synapses onto the terminals of Off cone bipolar cells (Fig. 6*B*). Under D_1-R blockade, the sustained excitatory component is greatly diminished (Fig. 6*C*), suggesting a loss of input from AII amacrine cells to Off cone bipolar cells.

Examining the inhibitory input to tOff-αRGCs under control conditions revealed a strong sustained disinhibition at light offset that showed weak surround antagonism (Fig. 6*B* and *E*) (Warwick et al., 2018). This disinhibition largely originates from AII amacrine cells, although other inhibitory cells may contribute (Manookin et al., 2008; Warwick et al., 2018). Under D_1-R blockade, disinhibition was greatly diminished for smaller spot sizes (in accordance with the diminished sustained excitation) and a gain of inhibition was observed for larger spot sizes (Fig. 6*C* and *E*). Consequently, disinhibition at light onset (following the disappearance of the dark spot) was observed for large spots (Fig. 6*C*), which could underlie the On responses observed in the spiking activity of tOff-αRGCs under D_1-R blockade (Fig. 4*C* and *E*). Additionally, this change from disinhibition to inhibition at light offset may explain why tOff-αRGCs with On responses reduced their sustained Off responses.

Under control conditions AII amacrine cells are thought to provide tonic inhibition to the tOff-αRGC that is then released at light offset (Manookin et al., 2008). The lack of disinhibition at light offset under D_1-R blockade suggests a loss of input from AII amacrine cells to the tOff-αRGC, in line with the loss of the sustained excitation that is also thought to be mediated via AII cells. Comparing the injected current needed to hold the cell at 0 mV revealed a significant decrease for tOff-αRGCs under D_1-R blockade (Fig. 6*F*). This could be the result of a more depolarised resting potential in the presence of the D_1-R antagonist, and/or increased input resistance due to loss of tonic inhibitory conductance. Indeed, we found that the input resistance was increased from 48.9 $\pm$ 7.2 mΩ to 98.5 $\pm$ 65.1 mΩ (mean $\pm$ SD) with the D_1-R antagonist ($P = 0.032$, Wilcoxon rank-sum test). Either way, our observation of reduced holding current could be caused by the loss of tonic inhibition from AII amacrine cells. While a loss of input from AII amacrine cells can explain the loss of disinhibition at light offset, it does not explain the gain of inhibition for large spot sizes. One possibility is that this gain of inhibition was previously masked by the strong disinhibition. Another possibility is that D_1-R blockade caused the tOff-αRGC to gain an additional inhibitory input in its surround receptive field (see Discussion).

Thus, D_1-R blockade had specific effects on the different synaptic components arriving onto the tOff-αRGC. Firstly, it reduced transient excitatory inputs derived from Off cone bipolar cells and weakened their surround antagonism. Secondly, it reduced inputs from the primary rod pathway and caused an increase in inhibition to occur at light offset for larger spot sizes, resulting in surround activation of tOff-αRGCs. In conclusion, dopamine appeared to affect distinct retinal pathways differently, and its role in shaping RGCs' centre–surround receptive fields is specific to individual RGC subtypes and the pathways underlying their responses.

Discussion

In this study we sought to investigate how dopamine shapes the receptive field properties of RGCs. We first show, using MEA recordings, that a dopamine receptor agonist can either strengthen or weaken an RGC's surround and does so in a subtype-specific manner. We then proceeded to study a specific genetically labelled RGC subtype, the tOff-αRGC. We observed that the dopamine receptor agonist apomorphine facilitates light responses to small stimuli, whereas dopamine receptor antagonists reduce them. Blockade of D_1-R revealed responses of opposite polarity (On responses) in response to large stimuli, characteristic of surround activation. Using voltage-clamp recordings, we showed that while D_1-R blockade weakened the surround of excitatory inputs, it enhanced the surround of inhibitory inputs, leading to disinhibition at light onset for large spot stimuli, which underlie the On response. Together, these data suggest that the role of dopamine in shaping receptive field properties of RGCs results from its specific effects on distinct retinal pathways.

Combining population and single-cell recordings to uncover subtype-specific effects of dopamine

Dopamine has long been reported to increase surround inhibition of RGCs (Jensen, 1991; Jensen & Daw, 1984, 1986). However, dopamine's effects on RGCs' receptive fields are likely to be far more complicated given what we know about its multiple functions, including modulating gap junctions and altering intrinsic cellular conductances (Bloomfield & Völgyi, 2009; Goel & Mangel, 2021; Roy & Field, 2019). The picture is further complicated by the fact that dopamine receptors are expressed on every major cell

type of the retina, including RGCs themselves, and that these receptors can be divided into two families that may have opposing effects (Witkovsky, 2004).

Using MEA recordings and clustering, we were able to group RGCs into functional subtypes. While we likely underestimated the number of subtypes, we did identify changes to receptive field structure that are consistent within clusters, which correspond to one or possibly multiple yet very similar RGC subtypes. Recording from hundreds of RGCs simultaneously, we could not optimally stimulate each RGC at its receptive field centre. Thus, for many cells the 'centre' stimulus may be slightly offset from the cell's receptive field centre (see example in Fig. 1*B*, bottom left) and therefore not elicit the optimal response. Moreover, non-linear dendritic integration can add to response variability, depending on the location of the stimulus on the cell's receptive field (Enroth-Cugell & Robson, 1966; Grimes et al., 2014; Ran et al., 2020). Using patch clamp recordings, we were then able to display a greater number of stimulus sizes that were exactly centred on the recorded cell, as well as use a contrast that elicited optimal responses for tOff-αRGCs (black spot on grey background; Warwick et al., 2018). These differences in the light stimuli may underlie some variability between MEA and patch clamp experiments. Importantly, our finding from the MEA recordings – enhanced responses to small stimuli with apomorphine – match those of tOff-αRGC targeted recordings, suggesting that cluster 15, the 'tOff-α cluster', either exclusively contains tOff-αRGCs, or at least that a large proportion are tOff-αRGCs. Our results show that the approach of large-scale population recordings, subsequent clustering of cells and targeting of known subtypes for detailed electrophysiological experiments can yield detailed results about underlying circuits.

Mechanisms of D_1-R and D_2-R activation in shaping tOff-αRGC responses

Despite D_1-R and D_2-R having opposing effects, we found some similarity between the effects of D_1-R and D_2-R blockers, as both reduced Off responses in tOff-αRGCs to small spot stimuli. Accordingly, apomorphine increased tOff-αRGC responses to small spot stimuli. Previously, dopamine was shown to enhance glutamate-gated currents in Off cone bipolar cells of the salamander retina via D_1-R (Maguire & Werblin, 1994). If the same mechanism exists in the mouse retina, this could explain the increased responses of tOff-αRGCs to small stimuli in the presence of the dopamine receptor agonist as well as the decreased responses under D_1-R blockade. However, another mechanism must be responsible for reducing responses to small spot stimuli during D_2-R blockade. Heterotypic gap-junctional coupling between rods and cones is regulated by dopamine via D_2-R, specifically the D_4 receptor (Li et al., 2013; Ribelayga et al., 2008). Blocking this receptor causes an increase in gap-junctional coupling between rods and cones (Bloomfield & Völgyi, 2009; Roy & Field, 2019) that will lower the photoreceptors' input resistance and may therefore weaken the signal that is transduced to bipolar cells. It may also weaken the antagonistic surround of the photoreceptors, which in turn affects the antagonistic surround of bipolar cells. This provides a potential explanation for the decrease in responses of tOff-αRGCs to small spot stimuli and loss of surround antagonism under D_2-R blockade.

A difference observed between D_1-R and D_2-R blockade was that only D_1-R blockade caused surround activation, as was evident by the On responses in tOff-αRGCs to large spot stimuli. Pharmacological blockade of the On pathway indicated that these On responses originate from the On pathway. Voltage-clamp experiments suggested that they were mediated by changes in inhibition, as under D_1-R blockade tOff-αRGCs exhibited inhibition at light offset and disinhibition at light onset for larger spot sizes.

Examining a dataset of single-cell RNA transcriptomics data revealed that tOff-αRGCs express *drd1* – the gene coding for the D_1-R receptor (Single Cell Portal (SCP), Broad Institute, based on Tran et al., 2019). This suggests the effects we detected with apomorphine and the D_1-R antagonist result (at least partly) from a direct activation of the tOff- αRGCs.

Variability in tOff-αRGC responses

Under D_1-R blockade, tOff-αRGC responses were quite variable, as the On response was observed in most, but not all, recorded cells, and the Off response tended to decrease only in these cells. This variability may originate from different locations of the recorded cells within the retina, since response properties of tOff-αRGC vary with their location along the ventral–dorsal retinal axis in a gradual manner (Heukamp et al., 2020; Warwick et al., 2018). Thus, although we only recorded from tOff-αRGCs located in the dorsal half of the retina, the circuits that underlie responses of tOff-αRGCs in the dorsal-most part and in the central part of the retina may differ.

Another possible source of variability can be the incubation times of the D_1-R blocker. Before recording we incubated the retina for 30 min in the D_1-R antagonist so that the long-term effects of D_1-R blockade, such as changes in gap-junctional coupling (Bloomfield & Völgyi, 2009; Goel & Mangel, 2021; Roy & Field, 2019), could take effect. The time it took to patch each tOff-αRGC varied and on some occasions more than one tOff-αRGC was patched in each retina piece, resulting in some cells

having longer incubations in the D_1-R antagonist. While dopamine acts in a paracrine fashion and could therefore be washed out in our experimental preparation, our results suggest that retinal dopamine levels are not zero as we did observe specific effects with dopamine receptor antagonists. We therefore assume that dopaminergic amacrine cells, like other retinal cells, remain active and continue to release dopamine in the *ex vivo* retinal preparation and that dopamine is not washed out.

Role of AII cells and D_1-Rs in shaping tOff-αRGC responses

Several lines of evidence suggest that under D_1-R blockade the tOff-αRGC loses input from the AII amacrine cell. Firstly, Off responses were reduced under D_1-R blockade compared with control conditions, but got stronger in the presence of L-AP4, which blocks the On pathway. This is in contrast to control conditions, where the On pathway is thought to enhance Off responses in tOff-αRGCs via AII disinhibition, and therefore Off responses are expected to be reduced in the presence of L-AP4. Secondly, when examining voltage-clamp recordings under D_1-R blockade, we observed a loss of sustained disinhibition arriving at the tOff-αRGC, as well as a loss of a sustained excitation, which is thought to arise from AII amacrine cell synapses onto Off cone bipolar cells. In accordance, when examining the spiking activity, the duration of the Off response is reduced in cells with On responses during D_1-R blockade compared with control tOff-αRGCs. Lastly, quantifying the current needed to hold the tOff-αRGC at 0 mV revealed a significant decrease under D_1-R blockade, possibly due to a loss of tonic inhibition from AII amacrine cells. AII amacrine cells express D_1 receptors (Nguyen-Legros et al., 1997) and are gap-junction coupled among themselves (Bloomfield & Völgyi, 2009). Could the loss of synaptic input from AII amacrine cells be the result of altered gap-junctional coupling among AII amacrine cells? AII amacrine cell gap-junctional coupling is triphasic – low in starlight, high in twilight and low again in daylight (Bloomfield & Völgyi, 2009). While it is clear that light adaptation is responsible for both increase in coupling from starlight to twilight and decrease in coupling from twilight to daylight, it is only decoupling at higher light levels that is thought to be mediated by dopamine (Roy & Field, 2019). This suggests that blocking D_1-R would increase coupling of AII amacrine cells, which may decrease their input resistance and therefore reduce their excitability and signalling onto tOff-αRGCs. In addition, since dopaminergic amacrine cells form perisomatic rings directly around AII amacrine cells (Debertin et al., 2015), it is possible that under control conditions the activity of the AII amacrine cells is enhanced by direct input from dopaminergic amacrine cells. Blocking D_1-R would have the opposite effect, reducing AII amacrine cell activity and consequently reducing input from AII amacrine cells to tOff-αRGCs. However, this would still not explain the gain of inhibition observed for larger spot sizes. A possible explanation for this phenomenon is that a reduction in disinhibition uncovers an inhibitory signal that may or may not have been there under control conditions. We do know that this inhibitory input is mediated by the On pathway and is therefore likely to originate from an On amacrine cell.

Conclusion

Previously, dopamine was thought to have a similar influence on all RGCs, namely to enhance their surround to increase spatial sensitivity at high illumination. At low illumination, when dopamine levels are low, the surround is comparatively weak to enhance spatial averaging and sensitivity to weak inputs (Rivlin-Etzion et al., 2018). As opposed to this simplified view, our findings demonstrate that a dopamine receptor agonist affects the centre–surround organisation of RGC receptive fields in a subtype-specific manner, via the differential effects it has on retinal pathways. Recent work reveals that centre–surround organisation does not merely control spatial integration, but may also contribute to more complex functions, such as motion detection (Ankri et al., 2020; Strauss et al., 2022). Thus, the differential effects dopamine has on different RGC subtypes may intricately shape visual processing to accommodate the visual requirements in different environmental conditions.

References

Ankri, L., Ezra-Tsur, E., Maimon, S. R., Kaushansky, N., & Rivlin-Etzion, M. (2020). Antagonistic center-surround mechanisms for direction selectivity in the retina. *Cell Reports*, **31**(5), 107608.

Baden, T., Berens, P., Franke, K., Román Rosón, M., Bethge, M., & Euler, T. (2016). The functional diversity of retinal ganglion cells in the mouse. *Nature*, **529**(7586), 345–350.

Barlow, H. B., Fitzhugh, R., & Kuffler, S. W. (1957). Change of organization in the receptive fields of the cat's retina during dark adaptation. *Journal of Physiology*, **137**(3), 338–354.

Bauer, B., Ehinger, B., & Åberg, L. (1980). [3H]-Dopamine release from the rabbit retina. *Albrecht v Graefes Arch klin exp Ophthal*, **215**(2), 71–78.

Beaudoin, D. L., Manookin, M. B., & Demb, J. B. (2008). Distinct expressions of contrast gain control in parallel synaptic pathways converging on a retinal ganglion cell. *Journal of Physiology*, **586**(22), 5487–5502.

Bloomfield, S. A., & Völgyi, B. (2009). The diverse functional roles and regulation of neuronal gap junctions in the retina. *Nature Reviews Neuroscience*, **10**(7), 495–506.

Brainard, D. H. (1997). The Psychophysics Toolbox. *Spatial Vision*, **10**(4), 433-436.

Chaffiol, A., Ishii, M., Cao, Y., & Mangel, S. C. (2017). Dopamine regulation of GABAA receptors contributes to light/dark modulation of the ON-cone bipolar cell receptive field surround in the retina. *Current Biology*, **27**(17), 2600–2609.e4.

Chichilnisky, E. J. (2001). A simple white noise analysis of neuronal light responses. *Network*, **12**(2), 199–213.

Debertin, G., Kántor, O., Kovács-Öller, T., Balogh, L., Szabó-Meleg, E., Orbán, J., Nyitrai, M., & Völgyi, B. (2015). Tyrosine hydroxylase positive perisomatic rings are formed around various amacrine cell types in the mammalian retina. *Journal of Neurochemistry*, **134**(3), 416–428.

Dedek, K., Pandarinath, C., Alam, N. M., Wellershaus, K., Schubert, T., Willecke, K., Prusky, G. T., Weiler, R., & Nirenberg, S. (2008). Ganglion cell adaptability: Does the coupling of horizontal cells play a role? *PLoS One*, **3**(3), e1714.

Demb, J. B., & Singer, J. H. (2012). Intrinsic properties and functional circuitry of the AII amacrine cell. *Visual Neuroscience*, **29**(1), 51–60.

Dunn, F. A., Doan, T., Sampath, A. P., & Rieke, F. (2006). Controlling the gain of rod-mediated signals in the Mammalian retina. *Journal of Neuroscience*, **26**(15), 3959–3970.

Dunn, F. A., Lankheet, M. J., & Rieke, F. (2007). Light adaptation in cone vision involves switching between receptor and post-receptor sites. *Nature*, **449**(7162), 603–606.

Enroth-Cugell, C., & Robson, J. G. (1966). The contrast sensitivity of retinal ganglion cells of the cat. *Journal of Physiology*, **187**(3), 517–552.

Farrow, K., Teixeira, M., Szikra, T., Viney, T. J., Balint, K., Yonehara, K., & Roska, B. (2013). Ambient illumination toggles a neuronal circuit switch in the retina and visual perception at cone threshold. *Neuron*, **78**(2), 325–338.

Farshi, P., Fyk-Kolodziej, B., Krolewski, D. M., Walker, P. D., & Ichinose, T. (2016). Dopamine D1 receptor expression is bipolar cell type-specific in the mouse retina. *Journal of Comparative Neurology*, **524**(10), 2059–2079.

Fein, A., & Szuts, E. Z. (1982). *Photoreceptors: Their Role in Vision*. books.google.com

Flood, M. D., & Eggers, E. D. (2021). Dopamine D1 and D4 receptors contribute to light adaptation in ON-sustained retinal ganglion cells. *Journal of Neurophysiology*, **126**(6), 2039–2052.

Flood, M. D., Moore-Dotson, J. M., & Eggers, E. D. (2018). Dopamine D1 receptor activation contributes to light-adapted changes in retinal inhibition to rod bipolar cells. *Journal of Neurophysiology*, **120**(2), 867–879.

Godley, B. F., & Wurtman, R. J. (1988). Release of endogenous dopamine from the superfused rabbit retina in vitro: effect of light stimulation. *Brain Research*, **452**(1–2), 393–395.

Goel, M., & Mangel, S. C. (2021). Dopamine-mediated circadian and light/dark-adaptive modulation of chemical and electrical synapses in the outer retina. *Frontiers in Cellular Neuroscience*, **15**, 647541.

Goldman, M. E., & Kebabian, J. W. (1984). Aporphine enantiomers. Interactions with D-1 and D-2 dopamine receptors. *Molecular Pharmacology*, **25**(1), 18–23.

Gong, S., Zheng, C., Doughty, M. L., Losos, K., Didkovsky, N., Schambra, U. B., Nowak, N. J., Joyner, A., Leblanc, G., Hatten, M. E., & Heintz, N. (2003). A gene expression atlas of the central nervous system based on bacterial artificial chromosomes. *Nature*, **425**(6961), 917–925.

Grimes, W. N., Schwartz, G. W., & Rieke, F. (2014). The synaptic and circuit mechanisms underlying a change in spatial encoding in the retina. *Neuron*, **82**(2), 460–473.

Herlinger, E., Jameson, R. F., & Linert, W. (1995). Spontaneous autoxidation of dopamine. *Journal of the Chemical Society, Perkin Transactions*, **2**(2), 259.

Herrmann, R., Heflin, S. J., Hammond, T., Lee, B., Wang, J., Gainetdinov, R. R., Caron, M. G., Eggers, E. D., Frishman, L. J., McCall, M. A., & Arshavsky, V. Y. (2011). Rod vision is controlled by dopamine-dependent sensitization of rod bipolar cells by GABA. *Neuron*, **72**(1), 101–110.

Heukamp, A. S., Warwick, R. A., & Rivlin-Etzion, M. (2020). Topographic variations in retinal encoding of visual space. *Annual Review of Vision Science*, **6**(1), 237–259.

Hoggarth, A., McLaughlin, A. J., Ronellenfitch, K., Trenholm, S., Vasandani, R., Sethuramanujam, S., Schwab, D., Briggman, K. L., & Awatramani, G. B. (2015). Specific wiring of distinct amacrine cells in the directionally selective retinal circuit permits independent coding of direction and size. *Neuron*, **86**(1), 276–291.

Hu, E. H., Pan, F., Völgyi, B., & Bloomfield, S. A. (2010). Light increases the gap junctional coupling of retinal ganglion cells. *Journal of Physiology*, **588**(Pt 21), 4145–4163.

Huberman, A. D., Manu, M., Koch, S. M., Susman, M. W., Lutz, A. B., Ullian, E. M., Baccus, S. A., & Barres, B. A. (2008). Architecture and activity-mediated refinement of axonal projections from a mosaic of genetically identified retinal ganglion cells. *Neuron*, **59**(3), 425–438.

Jensen, R., & Daw, N. (1984). Effects of dopamine antagonists on receptive fields of brisk cells and directionally selective cells in the rabbit retina. *Journal of Neuroscience*, **4**(12), 2972–2985.

Jensen, R. J. (1991). Involvement of glycinergic neurons in the diminished surround activity of ganglion cells in the dark-adapted rabbit retina. *Visual Neuroscience*, **6**(1), 43–53.

Jensen, R. J., & Daw, N. W. (1986). Effects of dopamine and its agonists and antagonists on the receptive field properties of ganglion cells in the rabbit retina. *Neuroscience*, **17**(3), 837–855.

Jouty, J., Hilgen, G., Sernagor, E., & Hennig, M. H. (2018). Non-parametric physiological classification of retinal ganglion cells in the mouse retina. *Frontiers in Cellular Neuroscience*, **12**, 481.

Karamanlis, D., & Gollisch, T. (2021). Nonlinear spatial integration underlies the diversity of retinal ganglion cell responses to natural images. *Journal of Neuroscience*, **41**(15), 3479–3498.

Kim, T., Shen, N., Hsiang, J. C., Johnson, K. P., & Kerschensteiner, D. (2020). Dendritic and parallel processing of visual threats in the retina control defensive responses. *Science Advances*, **6**(47), eabc9920.

Kothmann, W. W., Massey, S. C., & O'Brien, J. (2009). Dopamine-stimulated dephosphorylation of connexin 36 mediates AII amacrine cell uncoupling. *Journal of Neuroscience*, **29**(47), 14903–14911.

Koulen, P. (1999). Postnatal development of dopamine D1 receptor immunoreactivity in the rat retina. *Journal of Neuroscience Research*, **56**(4), 397–404.

Kreuz, T., Chicharro, D., Houghton, C., Andrzejak, R. G., & Mormann, F. (2013). Monitoring spike train synchrony. *Journal of Neurophysiology*, **109**(5), 1457–1472.

Kreuz, T., Mulansky, M., & Bozanic, N. (2015). SPIKY: A graphical user interface for monitoring spike train synchrony. *Journal of Neurophysiology*, **113**(9), 3432–3445.

Krieger, B., Qiao, M., Rousso, D. L., Sanes, J. R., & Meister, M. (2017). Four alpha ganglion cell types in mouse retina: Function, structure, and molecular signatures. *PLoS One*, **12**(7), e0180091.

Lee, S., Zhang, Y., Chen, M., & Zhou, Z. J. (2016). Segregated glycine-glutamate co-transmission from vGluT3 amacrine cells to contrast-suppressed and contrast-enhanced retinal circuits. *Neuron*, **90**(1), 27–34.

Li, H., Zhang, Z., Blackburn, M. R., Wang, S. W., Ribelayga, C. P., & O'Brien, J. (2013). Adenosine and dopamine receptors coregulate photoreceptor coupling via gap junction phosphorylation in mouse retina. *Journal of Neuroscience*, **33**(7), 3135–3150.

Maguire, G., & Werblin, F. (1994). Dopamine enhances a glutamate-gated ionic current in OFF bipolar cells of the tiger salamander retina. *Journal of Neuroscience*, **14**(10), 6094–6101.

Manookin, M. B., Beaudoin, D. L., Ernst, Z. R., Flagel, L. J., & Demb, J. B. (2008). Disinhibition combines with excitation to extend the operating range of the OFF visual pathway in daylight. *Journal of Neuroscience*, **28**(16), 4136–4150.

Masland, R. H. (2012). The neuronal organization of the retina. *Neuron*, **76**(2), 266–280.

Mazade, R. E., & Eggers, E. D. (2013). Light adaptation alters the source of inhibition to the mouse retinal OFF pathway. *Journal of Neurophysiology*, **110**(9), 2113–2128.

Mazade, R. E., & Eggers, E. D. (2016). Light adaptation alters inner retinal inhibition to shape OFF retinal pathway signaling. *Journal of Neurophysiology*, **115**(6), 2761–2778.

Mazade, R. E., & Eggers, E. D. (2020). Inhibitory components of retinal bipolar cell receptive fields are differentially modulated by dopamine D1 receptors. *Visual Neuroscience*, **37**, E01.

Mazade, R. E., Flood, M. D., & Eggers, E. D. (2019). Dopamine D1 receptor activation reduces local inner retinal inhibition to light-adapted levels. *Journal of Neurophysiology*, **121**(4), 1232–1243.

Münch, T. A., da Silveira, R. A., Siegert, S., Viney, T. J., Awatramani, G. B., & Roska, B. (2009). Approach sensitivity in the retina processed by a multifunctional neural circuit. *Nature Neuroscience*, **12**(10), 1308–1316.

Muresan, Z., & Besharse, J. C. (1993). D2-like dopamine receptors in amphibian retina: Localization with fluorescent ligands. *Journal of Comparative Neurology*, **331**(2), 149–160.

Murphy, G. J., & Rieke, F. (2006). Network variability limits stimulus-evoked spike timing precision in retinal ganglion cells. *Neuron*, **52**(3), 511–524.

Murphy, G. J., & Rieke, F. (2008). Signals and noise in an inhibitory interneuron diverge to control activity in nearby retinal ganglion cells. *Nature Neuroscience*, **11**(3), 318–326.

Nguyen-Legros, J., Simon, A., Caillé, I., & Bloch, B. (1997). Immunocytochemical localization of dopamine D1 receptors in the retina of mammals. *Visual Neuroscience*, **14**(3), 545–551.

Nguyen-Legros, J., Versaux-Botteri, C., & Vernier, P. (1999). Dopamine receptor localization in the mammalian retina. *Molecular Neurobiology*, **19**(3), 181–204.

Ogata, G., Stradleigh, T. W., Partida, G. J., & Ishida, A. T. (2012). Dopamine and full-field illumination activate D1 and D2-D5-type receptors in adult rat retinal ganglion cells. *Journal of Comparative Neurology*, **520**(17), 4032–4049.

Pachitariu, M., Steinmetz, N. A., & Colonell, J. (2018). *Kilosort2*. https://github.com/MouseLand/

Pachitariu, M., Steinmetz, N., Kadir, S., Carandini, M., & Harris, K. D. (2016). Kilosort: realtime spike-sorting for extracellular electrophysiology with hundreds of channels. *BioRxiv*.

Pang, J.-J., Gao, F., & Wu, S. M. (2003). Light-evoked excitatory and inhibitory synaptic inputs to ON and OFF alpha ganglion cells in the mouse retina. *Journal of Neuroscience*, **23**(14), 6063–6073.

Pearson, J. T., & Kerschensteiner, D. (2015). Ambient illumination switches contrast preference of specific retinal processing streams. *Journal of Neurophysiology*, **114**(1), 540–550.

Pelli, D. G. (1997). The VideoToolbox software for visual psychophysics: transforming numbers into movies. *Spatial Vision*, **10**(4), 437–442.

Pérez-Fernández, V., Milosavljevic, N., Allen, A. E., Vessey, K. A., Jobling, A. I., Fletcher, E. L., Breen, P. P., Morley, J. W., & Cameron, M. A. (2019). Rod photoreceptor activation alone defines the release of dopamine in the retina. *Current Biology*, **29**(5), 763–774.e5.

Ran, Y., Huang, Z., Baden, T., Schubert, T., Baayen, H., Berens, P., Franke, K., & Euler, T. (2020). Type-specific dendritic integration in mouse retinal ganglion cells. *Nature Communications*, **11**(1), 2101.

Ribelayga, C., Cao, Y., & Mangel, S. C. (2008). The circadian clock in the retina controls rod-cone coupling. *Neuron*, **59**(5), 790–801.

Rivlin-Etzion, M., Grimes, W. N., & Rieke, F. (2018). Flexible neural hardware supports dynamic computations in retina. *Trends in Neuroscience*, **41**(4), 224–237.

Rivlin-Etzion, M., Zhou, K., Wei, W., Elstrott, J., Nguyen, P. L., Barres, B. A., Huberman, A. D., & Feller, M. B. (2011). Transgenic mice reveal unexpected diversity of on-off direction-selective retinal ganglion cell subtypes and brain structures involved in motion processing. *Journal of Neuroscience*, **31**(24), 8760–8769.

Rossant, C., & Harris, K. D. (2013). Hardware-accelerated interactive data visualization for neuroscience in Python. *Frontiers in Neuroinformatics*, **7**, 36.

Rossant, C., Kadir, S. N., Goodman, D. F. M., Schulman, J., Hunter, M. L. D., Saleem, A. B., Grosmark, A., Belluscio, M., Denfield, G. H., Ecker, A. S., Tolias, A. S., Solomon, S., Buzsaki, G., Carandini, M., & Harris, K. D. (2016). Spike sorting for large, dense electrode arrays. *Nature Neuroscience*, **19**(4), 634–641.

Roy, S., & Field, G. D. (2019). Dopaminergic modulation of retinal processing from starlight to sunlight. *Journal of Pharmacological Sciences*, **140**(1), 86–93.

Shapley, R., & Enroth-Cugell, C. (1984). Chapter 9 Visual adaptation and retinal gain controls. *Progress in Retinal Research*, **3**, 263–346.

Strauss, S., Korympidou, M. M., Ran, Y., Franke, K., Schubert, T., Baden, T., Berens, P., Euler, T., & Vlasits, A. L. (2022). Center-surround interactions underlie bipolar cell motion sensitivity in the mouse retina. *Nature Communications*, **13**(1), 5574.

Szikra, T., Trenholm, S., Drinnenberg, A., Jüttner, J., Raics, Z., Farrow, K., Biel, M., Awatramani, G., Clark, D. A., Sahel, J. A., Silveira, da R. A., & Roska, B. (2014). Rods in daylight act as relay cells for cone-driven horizontal cell-mediated surround inhibition. *Nature Neuroscience*, **17**(12), 1728–1735.

Tikidji-Hamburyan, A., Reinhard, K., Seitter, H., Hovhannisyan, A., Procyk, C. A., Allen, A. E., Schenk, M., Lucas, R. J., & Münch, T. A. (2015). Retinal output changes qualitatively with every change in ambient illuminance. *Nature Neuroscience*, **18**(1), 66–74.

Tikidji-Hamburyan, A., Reinhard, K., Storchi, R., Dietter, J., Seitter, H., Davis, K. E., Idrees, S., Mutter, M., Walmsley, L., Bedford, R. A., Ueffing, M., Ala-Laurila, P., Brown, T. M., Lucas, R. J., & Münch, T. A. (2017). Rods progressively escape saturation to drive visual responses in daylight conditions. *Nature Communications*, **8**(1), 1813.

Tran, N. M., Shekhar, K., Whitney, I. E., Jacobi, A., Benhar, I., Hong, G., Yan, W., Adiconis, X., Arnold, M. E., Lee, J. M., Levin, J. Z., Lin, D., Wang, C., Lieber, C. M., Regev, A., He, Z., & Sanes, J. R. (2019). Single-cell profiles of retinal ganglion cells differing in resilience to injury reveal neuroprotective genes. *Neuron*, **104**(6), 1039–1055.e12.

van Wyk, M., Wässle, H., & Taylor, W. R. (2009). Receptive field properties of ON- and OFF-ganglion cells in the mouse retina. *Visual Neuroscience*, **26**(3), 297–308.

Veruki, M. L. (1997). Dopaminergic neurons in the rat retina express dopamine D2/3 receptors. *European Journal of Neuroscience*, **9**(5), 1096–1100.

Veruki, M. L., & Wässle, H. (1996). Immunohistochemical localization of dopamine D receptors in rat retina. *European Journal of Neuroscience*, **8**(11), 2286–2297.

Vlasits, A. L., Bos, R., Morrie, R. D., Fortuny, C., Flannery, J. G., Feller, M. B., & Rivlin-Etzion, M. (2014). Visual stimulation switches the polarity of excitatory input to starburst amacrine cells. *Neuron*, **83**(5), 1172–1184.

Wang, F., Li, E., De, L., Wu, Q., & Zhang, Y. (2021). OFF-transient alpha RGCs mediate looming triggered innate defensive response. *Current Biology*, **31**(11), 2263–2273.e3.

Warwick, R. A., Kaushansky, N., Sarid, N., Golan, A., & Rivlin-Etzion, M. (2018). Inhomogeneous encoding of the visual field in the mouse retina. *Current Biology*, **28**(5), 655–665.e3.

Warwick, R. A., Riccitelli, S., Heukamp, A. S., Yaakov, H., Ankri, L., Mayzel, J., Gilead, N., Parness-Yossifon, R., & Rivlin-Etzion, M. (2022). Top-down modulation of the retinal code via histaminergic neurons of the hypothalamus. *BioRxiv*. Advance online publication. https://doi.org/10.1101/2022.04.26.489509

Wei, W., Elstrott, J., & Feller, M. B. (2010). Two-photon targeted recording of GFP-expressing neurons for light responses and live-cell imaging in the mouse retina. *Nature Protocols*, **5**(7), 1347–1352

Witkovsky, P. (2004). Dopamine and retinal function. *Documenta Ophthalmologica*, **108**(1), 17–39.

Xin, D., & Bloomfield, S. A. (1999). Dark- and light-induced changes in coupling between horizontal cells in mammalian retina. *Journal of Comparative Neurology*, **405**(1), 75–87.

Additional information

Data availability statement

All relevant data are presented in the figures and the supplementary information. Data are available on request from the lead author. The supplementary information can be found on our lab's GitHub repository under the following address: https://github.com/RivlinLab/Dopamine_Retina

Competing interests

The authors declare no competing financial interests.

Author contributions

All authors designed experiments. S.R. performed MEA experiments. A.S.H. analysed MEA experiments. R.A.W. performed patch clamp experiments and analysis. R.A.W, A.S.H. and M.R.-E. wrote the manuscript with input from S.R. All authors edited the manuscript. All authors have read and approved the final version of this manuscript and agree to be accountable for all aspects of the work in ensuring that questions related to the accuracy or integrity of any part of the work are appropriately investigated and resolved. All persons designated as authors qualify for authorship, and all those who qualify for authorship are listed.

Funding

This project has received funding from the I-CORE (51/11), the Minerva Foundation with funding from the Federal German Ministry for Education and Research, the ISF Foundation (1396/15 and 2449/20), the European Research Council under the European Union's Horizon 2020 research and innovation program (grant agreement no. 757732). We also acknowledge support from the Sagol Weizmann-MIT Bridge Program, Dr and Mrs Alan Leshner, the Lubin-Schupf Fund for Women

in Science, the Charles and David Wolfson Charitable Trust, Rolf Wiklund and Alice Wiklund Parkinson's disease research fund, Consolidated Anti-Aging Foundation, Dr Daniel C. Andreae and Ms Lois Pope. R.A.W. was supported by the Dean of Faculty fellowship and the Koshland Foundation at Weizmann Institute of Science. A.S.H. was supported by the Minerva Fellowship. S.R. was supported by the Dean of Faculty fellowship. M.R.-E. is incumbent of the Sara Lee Schupf Family Chair.

Acknowledgements

We thank members of the Rivlin lab and Batel Rephael for fruitful discussions.

Keywords

apomorphine, centre–surround receptive field, dopamine, multielectrode array, retina, retinal ganglion cells, transient Off-αRGC

Supporting information

Additional supporting information can be found online in the Supporting Information section at the end of the HTML view of the article. Supporting information files available:

Statistical Summary Document
Peer Review History
Supporting Information